A nonlinear repair technique for the MPFA-D scheme in single-phase flow problems and heterogeneous and anisotropic media

Reis de Souza, Artur Castiel; Elisiário de Carvalho, Darlan Karlo; de Moura Cavalcante, Túlio; Licapa Contreras, Fernando Raul; Edwards, Michael G.; Lyra, Paulo Roberto Maciel

DOI
10.1016/j.jcp.2024.112759

Publication date
2024

Document Version
Final published version

Published in
Journal of Computational Physics

Citation (APA)
Reis de Souza, A. C., Elisiário de Carvalho, D. K., de Moura Cavalcante, T., Licapa Contreras, F. R., Edwards, M. G., & Lyra, P. R. M. (2024). A nonlinear repair technique for the MPFA-D scheme in single-phase flow problems and heterogeneous and anisotropic media. *Journal of Computational Physics*, *501*, Article 112759. https://doi.org/10.1016/j.jcp.2024.112759

Journal of Computational Physics 501 (2024) 112759

Contents lists available at ScienceDirect

Journal of Computational Physics

journal homepage: www.elsevier.com/locate/jcp

A nonlinear repair technique for the MPFA-D scheme in single-phase flow problems and heterogeneous and anisotropic media

Artur Castiel Reis de Souza [b,*], Darlan Karlo Elisiário de Carvalho [e], Túlio de Moura Cavalcante [c], Fernando Raul Licapa Contreras [d], Michael G. Edwards [a], Paulo Roberto Maciel Lyra [e]

[a] Zienkiewicz Centre for Computational Engineering, Swansea University, Bay Campus, Swansea, SA1 8EN, UK
[b] Delft Institute of Applied Mathematics, Delft University of Technology, Mekelweg 4, 2628 CD, Delft, Netherlands
[c] Civil Engineering Department, Universidade Federal de Pernambuco, Av. da Arquitetura, S/N, CEP 50740-550 Recife, Brazil
[d] Núcleo de Tecnologia, Centro Acadêmico do Agreste, Universidade Federal de Pernambuco, Rodovia BR 104, KM 59 s/n: 55002-970, Caruaru, PE, Brazil
[e] Mechanical Engineering Department, Universidade Federal de Pernambuco, Av. da Arquitetura, S/N, CEP 50740-550 Recife, Brazil

ARTICLE INFO

Keywords:
Flux limited splitting (FLS)
Non-linear repair technique
Discrete maximum principle (DMP)
Heterogeneous and anisotropic media
Unstructured meshes

ABSTRACT

A novel Flux Limited Splitting (FLS) non-linear Finite Volume (FV) method for families of linear Control Volume Distributed Multi Point Flux Approximation (CVD-MPFA) schemes is presented. The new formulation imposes a local discrete maximum principal (LDMP) which ensures that the discrete solution is free of spurious oscillations. The FLS scheme can be seen as a natural extension of the M-Matrix Flux Splitting method that splits the MPFA flux components in terms of the Two-Point Flux Approximation (TPFA) flux and Cross Diffusion Terms (CDT), with the addition of a dynamically computed relaxation parameter to the CDT that identifies and locally corrects the regions where the LDMP is violated. Moreover, the whole non-linear procedure was devised as a series of simple straightforward matrix operations. The methodology is presented considering the Multi-Point Flux Approximation with a Diamond (MPFA-D) in what we call the FLS + MPFA-D formulation which is tested using a series of challenging benchmark problems. For all test cases, the FLS repair technique imposes the LDMP and eliminates the spurious oscillations induced by the original MPFA-D method.

1. Introduction

In many branches of engineering and science a diffusion operator arises, common examples include the heat flow, mass transport, electrostatics and flow through porous media [4,26,15]. For instance, in the context of fluid flow in porous media modeling, the pressure equation involves an analogous diffusion like operator. The analogous diffusion coefficient is proportional to the permeability of the media, which is, in general, represented by an anisotropic and heterogeneous, possibly discontinuous, tensor. Among the many important properties of numerical methods, accuracy, cost-efficiency and allowing arbitrary diffusion tensors are key features.

* Corresponding author.
E-mail address: a.castielreisdesouza@tudelft.nl (A.C.R. de Souza).

https://doi.org/10.1016/j.jcp.2024.112759
Received 5 June 2023; Received in revised form 23 November 2023; Accepted 6 January 2024

Available online 17 January 2024

In the context of management of subsurface oil reservoirs, a diffusion operator often appears at the center of standard petroleum reservoir simulators, commonly used by tools such as history matching and optimization which make broad use of simulations. Core to the most common standard simulators, lies the Two-Point Flux Approximation (TPFA) scheme. The TPFA method with harmonic mean of the local interface permeabilities can lead to a consistent locally conservative flux-continuous finite-volume method provided the resulting tensor is strictly diagonal. The main advantages of TPFA over other flux approximation schemes are due to the pressure equation having a symmetric M-matrix of minimal bandwidth making the method highly efficient. The M-matrix ensures the scheme satisfies the Local Discrete Maximum Principle (LDMP) [21] so yielding solutions free from spurious oscillations. However, this scheme fails to produce consistent solution for non k-orthogonal grids and for media with full permeability tensors. The Multi-Point Flux Approximation (MPFA) family of consistent methods for full-tensor problems on non k-orthogonal grids were presented in [12,1,19]. These schemes were further developed [13,20,8,23,9,10] and employed in several different applications [34,16,7]. As an example, in the petroleum reservoir simulation context, the spurious oscillations in pressure caused by the inability to ensure a LDMP may lead to the appearance of false gas pockets when the pressure drops below the bubble point and oil moving from low to high pressure zones [37]. As with all linear finite-volume and finite element methods, both CVD-MPFA schemes with full pressure support (FPS) e.g. [21,23] and earlier Triangle Pressure Support (TPS) methods each have conditional M-Matrices and therefore a conditional LDMP. Consequently, media with strong anisotropic full-tensors can cause these methods to violate the LDMP, however only the earlier TPS methods induce severe spurious oscillations. In [20,21] it is shown that the TPS methods suffer from decoupling for such problems, while the FPS formulations prevent decoupling and yield results free from severe non-physical oscillations at the mesh level, even though these methods can lack a formal local LDMP for such cases. We also note that all linear methods have a conditional LDMP and consequently lack a formal LDMP for such cases.

CVD-MPFA methods remain the popular choice for reservoir simulation, providing optimal consistent flux-continuous approximations on structured and unstructured grids and depend on a single degree of freedom per control-volume per flow variable. The methods apply to problems involving media with abrupt variation in permeability fields, convoluted geometries such as inclined laminated layers, channels and fractures [10,14].

Interest in formulations that are guaranteed to yield results that are free of non-physical oscillations has led to development of Non-Linear Finite Volume methods (NL-FV) which satisfy the DMP or, at least, produce monotone solutions, for arbitrary full-tensor permeability fields and general non k-orthogonal unstructured meshes [28,29,43,5,24,37,11,6,35,30]. Related non-linear schemes involve repair techniques. The main idea in these methods is to add a non-linear iterative procedure in order to improve or mitigate problems related to the loss of the LDMP property that can occur whenever using linear methods such as MPFA methods to model strongly anisotropic problems. We highlight the work of [17] who presented the M-Matrix Flux Splitting method, an iterative technique which is applied to the CVD-MPFA formulation, but also applies to other FV and FEM methods. The CVD-MPFA flux is split into a TPFA flux and a cross-diffusion flux, the resulting matrices are used to define a semi-implicit iterative technique, where iteration is performed by using the M-Matrix of the TPFA scheme as an iterative driver operating acting on the new iterate while the cross terms are calculated at the previous iterate level, with splitting at the flux level ensuring conservation is maintained at each iteration level. This method was later modified by introducing pressure limiters capable of improving the loss of monotonicity while maintaining mass conservation. [31,33]. In the finite elements context, the work of [27] inspired by the Flux Corrected Transport (FCT) approach devised a repair technique that splits the flux approximation in the diffusive and anti-diffusive fluxes and performs a flux limitation to reinforce a DMP. The work of Cavalcante et al. [6] takes advantages of these ideas and performs a limitation based on a Gauss–Seidel decomposition to limit the cross diffusion.

In the present paper, we introduce a general repair technique based on a flux limiting strategy for linear CVD-MPFA methods capable of restoring the LDMP whilst maintaining mass conservation. The method involves splitting the flux into a TPFA flux and a cross diffusion flux as presented in [17], however a relaxation parameter is included to bound the cross diffusion flux influence. An algorithm similar to [6] is proposed to calculate the limiter parameters to ensure, at each step of the iterative procedure the solution, that is closer to a bounded solution that satisfies the DMP. In our novel approach, the limiter algorithm is based on the M-Matrix Splitting [17], ensuring convergence for the most challenging problems. In addition, an algorithm to find the most suitable initial solution for the iterative procedure is also proposed. Our proposed method is tested using the Flux Limited Splitting applied to the Multi-Point Flux Approximation with a Diamond Stencil (MPFA-D) [23,9], which is a full pressure support method, known for producing accurate results even for challenging diffusion problems with strongly anisotropic heterogeneous media and distorted meshes.

The article is organized as follows: in the first three sections, we introduce the mathematical model and the numerical scheme we have developed to solve it. In Sections 2 and 3, we describe the steady-state diffusion equations that describe the single-phase flow in porous media, as well as the numerical formulation of the classical linear TPFA and the MPFA-D methods, and the theory of the flux splitting technique. In section 3, we present some numerical examples used to show the accuracy and robustness of our formulation and, in section 4, we present conclusions.

2. Mathematical model and numerical formulation

In the present article, we consider the steady-state single-phase of an incompressible and isothermal fluid-flow through an incompressible media Ω which is given, by:

$$\vec{\nabla} \cdot \vec{v} = Q \quad \text{with} \quad \vec{v} = -\frac{\overline{K}}{\mu} \nabla p \tag{1}$$

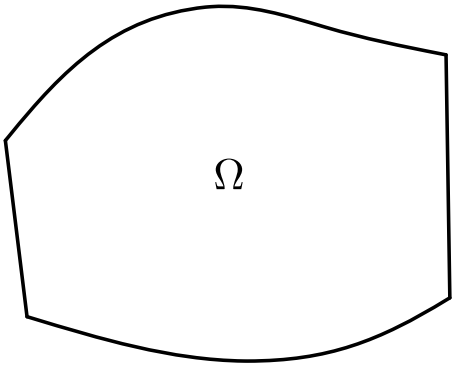

(a) Physical domain Ω.

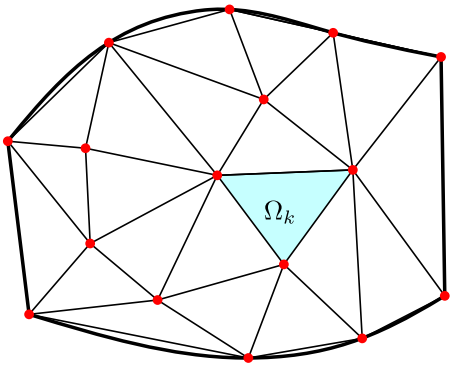

(b) General Control Volume Ω_k (light blue) in discrete representation of the mesh used to spatially discretize Ω .

Fig. 1. Representation of a physical domain and its discretization.

where $\vec{v}$ denotes a diffusive flux, in this case, Darcy's flux, with $\overline{K}$ representing the symmetric rock permeability tensor, μ is the fluid viscosity, p is the fluid pressure; and Q is the source or sink term. Here, the capillarity and gravity effects were neglected.

The associated boundary conditions are defined as:

$$\begin{cases} p = g_D & \text{on} \quad \partial\Omega_D \\ \vec{v} \cdot \vec{N} = g_N & \text{in} \quad \partial\Omega_N \end{cases} \tag{2}$$

where $\vec{N}$ represents the normal area vector, g_D and g_N denote, respectively, prescribed pressure and flux, defined on $\partial\Omega_D$, on $\partial\Omega_N$ i.e. Dirichlet and Neumann boundaries with, $\partial\Omega_N \cap \partial\Omega_D = \varnothing$.

Two important features distinguish the cell-centred family of Finite Volume methods. The first is the partitioning of the physical domain into smaller volumes with scalar unknowns (e.g. pressures) associated with CVs of that grid, while the second is the conservative form of the equations [38,42]. Before moving on to the definitions of the flux approximation, it is important to formally establish some terms that will be used extensively in this work.

Mesh or Grid (Ω^f or Ω): The mesh is a spatial discretization of the physical domain Ω. See Fig. 1. For the sake of simplicity Ω and $\partial\Omega$ are also used to denote the computational domain, and its boundaries.
Volume (Ω_k): The computational domain is subdivided in a set of $\{\Omega_k\}_{k=1}^{n_v}$ of n_v volumes or control volumes.
Face or Surface (Γ_j): The set of non overlapping faces is defined such that $\{\Gamma_j\}_{j=1}^{n_f} = \partial\Omega_i \cap \partial\Omega_j \ \forall(\Omega_i, \Omega_j) \in \Omega$ with $i \neq j$ and $\Gamma_j \neq \emptyset$.
Volume Boundaries ($\partial\Omega_k$): The boundaries of a control volume Ω_k is a set defined as $\partial\Omega_k = \{\Gamma_j \in \Omega_k\}$.

Integration of equation (1) over the domain Ω yields:

$$\int_\Omega \vec{\nabla} \cdot \vec{v} dV = \int_\Omega Q dV \tag{3}$$

Discretizing the domain Ω into n_v control volumes allows us to express equation (3) for a general control volume Ω_k as follows:

$$\int_{\Omega_k} \vec{\nabla} \cdot \vec{v} dV = \int_{\Omega_k} Q dV \tag{4}$$

A semi-discrete version of Equation (3) is found by the summing Equation (4) for all the control volumes of the domain Ω:

$$\sum_{\forall\Omega_k \in \Omega} \int_{\Omega_k} \vec{\nabla} \cdot \vec{v} dV = \sum_{\forall\Omega_k \in \Omega} \int_{\Omega_k} Q dV \tag{5}$$

Applying the Divergence Theorem to the LHS of equation (4), we obtain:

$$\int_{\partial\Omega_k} \vec{v} \cdot \vec{n} dA = \int_{\Omega_k} Q dV \tag{6}$$

Using the Mean Value Theorem applied to the LHS and RHS of Equation (6), we obtain:

$$\int_{\partial\Omega_k} \vec{v} \cdot \vec{n} dA = \sum_{\Gamma_j \in \partial\Omega_k} \vec{v} \cdot \vec{N})_{\Gamma_k} \quad \text{and} \quad \int_{\Omega_k} Q dV = \bar{Q}_k \Omega_k \tag{7}$$

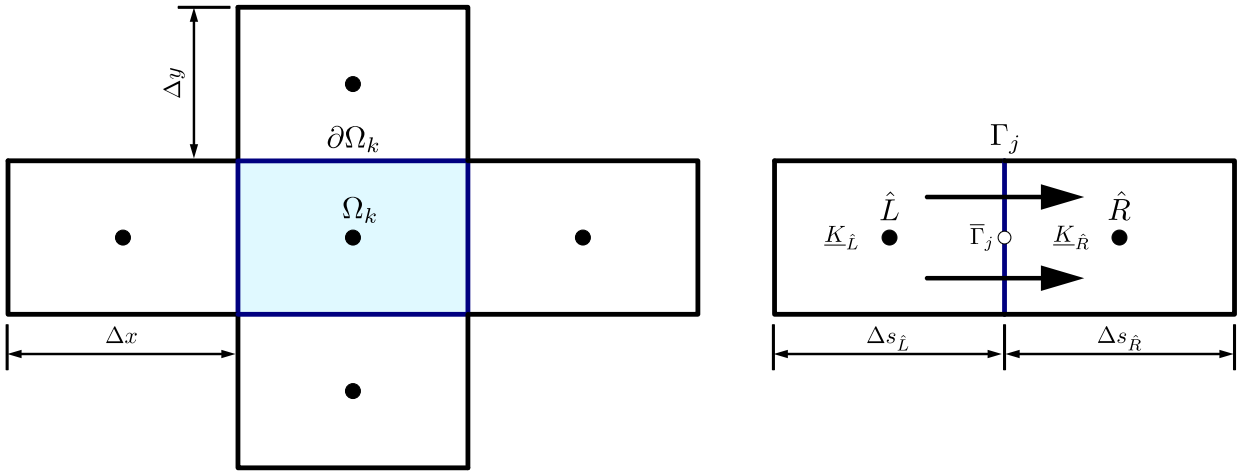

Fig. 2. Section of a k-orthogonal two-dimensional mesh used to derive the TPFA fluxes across the control surfaces $\partial\Omega_j$ (blue) of an arbitrary control volume Ω_k (light blue) in a 2-D domain. (For interpretation of the colours in the figure(s), the reader is referred to the web version of this article.)

We use the results in Equation (7) to find a discrete version of Equation (6).

$$\sum_{\Gamma_j \in \partial\Omega_k} (\vec{v} \cdot \vec{N})_{\Gamma_k} = \bar{Q}_k \Omega_k \tag{8}$$

where $\vec{v}_{\Gamma_k}$ stands for the mean velocity approximated on an arbitrary face Γ_k and the respective $\vec{N}_{\Gamma_k}$ the normal area vector in $\partial\Omega_k$, and where $\bar{Q}_k$ represents the mean value of the source/sink term, defining the concept of mass conservation at the discrete (mesh) level.

Definition 2.1. A numerical scheme is locally conservative if:

$$\sum_{\Gamma_j \in \partial\Omega_k} (\vec{v} \cdot \vec{N})_{\Gamma_j} = \bar{Q}_k \Omega_k \quad \forall \Omega_k \in \Omega \tag{9}$$

where the respective discrete Darcy-fluxes calculated for the control volumes to the left L and to the right R of Γ_j must satisfy:

$$(\vec{v} \cdot \vec{N})^L_{\Gamma_j} + (\vec{v} \cdot \vec{N})^R_{\Gamma_j} = 0 \quad \forall \Gamma_j \in \Gamma \tag{10}$$

2.1. Linear two-point flux approximation

Let us consider a section of a k-orthogonal two-dimensional mesh as shown in Fig. 2. For a fluid of unitary viscosity $\mu = 1$, and assuming that a control volume Ω_k is subjected to a pressure gradient along the x and y-axes, we can calculate the fluxes at the control surfaces $\partial\Omega_k$. The standard TPFA flux expression across a face Γ_j shared by two adjacent control volumes on the left L and on the right R, with corresponding centroids represented by $\hat{L}$, and $\hat{R}$ is defined as:

$$(\vec{v} \cdot \vec{N})_{\Gamma_j} = -\frac{2K_{L_{ss}} K_{R_{ss}}}{K_{L_{ss}} \Delta s_{\hat{R}} + K_{R_{ss}} \Delta s_{\hat{L}}} |\Gamma_j| (p_{\hat{R}} - p_{\hat{L}}) \tag{11}$$

Note that this approximation is only consistent for k-orthogonal grids because the tangential components of the permeability tensor are always omitted by this approximation. Thus, if $\overline{K}$ is not aligned with the main axis, crucial information is lost in the approximation. Consequently when applied to non k-orthogonal grids the two-point flux approximation is inconsistent and suffers from an $O(1)$ (zeroth order) error that does not reduce when the mesh is refined [20].

2.2. Multi-point flux approximation with a diamond stencil (MPFA-D)

The Multi-Point Flux Approximation with a Diamond stencil is a non-orthodox member of the family of CVD-MPFA schemes. It was first developed by Gao and Wu [23] and brought to the multiphase flow context by Contreras et al. [9]. Like other methods in the MPFA family, the MPFA-D was devised to tackle limitations of the standard Two-Point Flux Approximation (TPFA). Similar to the MPFA-FPS [22], the diamond method employs a full pressure support for each control volume of the discrete domain. Hence, this scheme does not suffer from decoupled solution modes and can produce well-behaved and consistent solutions with significantly less visible spurious oscillations when compared to the earlier CVD-MPFA methods. The MPFA-D will be adopted to introduce the proposed nonlinear repair technique, which can be extended for the whole MPFA family, in two or three dimensions.

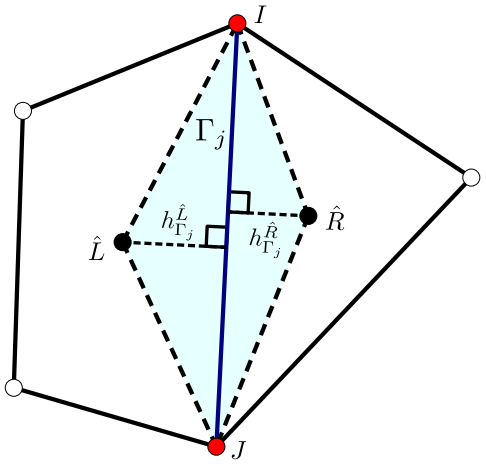

Fig. 3. Diamond stencil (light blue region) of the MPFA-D is created by connecting the centroids of two adjacent control volumes $\hat{L}$ and $\hat{R}$ with the nodes I and J that comprise a shared face Γ_j (dark blue).

The MPFA-D flux expression is also derived based on the hypotheses that fluxes are unique and continuous across different control volumes. Let us consider a fragment of a non k-orthogonal two-dimensional mesh as illustrated in Fig. 3. The diamond region is formed by connecting the centroids of two adjacent control volumes to the nodes I and J that comprise a shared face Γ_j creating two triangles. The unique MPFA-D flux over any surface Γ_j is defined as:

$$(\vec{v}\cdot\vec{N})_{\Gamma_j} \simeq \tau_{\Gamma_j}[p_{\hat{R}} - p_{\hat{L}} - \nu_{\Gamma_j}(p_J - p_I)] \tag{12}$$

The scalar transmissibility coefficient τ_{Γ_j} and the non-dimensional tangential ν_{Γ_j} in Equation (12) are defined as:

$$\tau_{\Gamma_j} = -|\Gamma_j|\frac{K^n_{\Gamma_j(L)}K^n_{\Gamma_j(R)}}{K^n_{\Gamma_j(L)}h^{\hat{R}}_{\Gamma_j} + K^n_{\Gamma_j(R)}h^{\hat{L}}_{\Gamma_j}} \tag{13}$$

$$\nu_{\Gamma_j} = \frac{\vec{\Gamma}_j\cdot\overrightarrow{\hat{L}\hat{R}}}{|\Gamma_j|^2} - \frac{1}{|\Gamma_j|}\left(\frac{K^t_{\Gamma_j(L)}}{K^n_{\Gamma_j(L)}}h^{\hat{L}}_{\Gamma_j} + \frac{K^t_{\Gamma_j(R)}}{K^n_{\Gamma_j(R)}}h^{\hat{R}}_{\Gamma_j}\right) \tag{14}$$

where $h^{\hat{L}}_{\Gamma_j}$ and $h^{\hat{R}}_{\Gamma_j}$ represent the height of the left $\hat{L}_{\Gamma_j}$ and right $\hat{L}_{\Gamma_j}$ element as depicted on pictures 3.

The normal $K^n_{\Gamma_j(el)}$ and tangential $K^t_{\Gamma_j(el)}$ components of the permeability tensor are defined, as:

$$K^n_{\Gamma_j(el)} = \frac{\vec{N}^T_{\Gamma_j}\underline{K}_{\Gamma_j(el)}\vec{N}_{\Gamma_j}}{|\Gamma_j|^2} \tag{15}$$

$$K^t_{\Gamma_j(el)} = \frac{\vec{N}^T_{\Gamma_j}\underline{K}_{\Gamma_j(el)}\vec{\Gamma}_j}{|\Gamma_j|^2} \tag{16}$$

where the superscript T represent the transpose operation and $\vec{\Gamma}_j$ represents the vector connecting the two nodes that comprise Γ_j. The MPFA-D flux for a control volume subjected to Dirichlet boundary conditions is given by the following expression:

$$(\vec{v}\cdot\vec{N})_{\Gamma_j} \simeq -\frac{K^n_{\Gamma_j}}{h^{\hat{L}}_{\Gamma_j}|\Gamma_j|}\left[(-\overrightarrow{J\hat{L}}\cdot\vec{\Gamma}_j)g_D(I) + \overrightarrow{I\hat{L}}\cdot\vec{\Gamma}_j g_D(J) - p_{\hat{L}}|IL|^2\right] - K^t_{\Gamma_j}\left(g_D(J) - g_D(I)\right) \tag{17}$$

where $g_D(I)$ and $g_D(J)$ are prescribed pressures on node I and J, respectively.

The flux expression for control volumes subjected to Neumann boundary conditions is defined as:

$$(\vec{v}\cdot\vec{N})_{\Gamma_j} = g_D|\Gamma_j| \tag{18}$$

where g_D represents the prescribed flux over Γ_j.

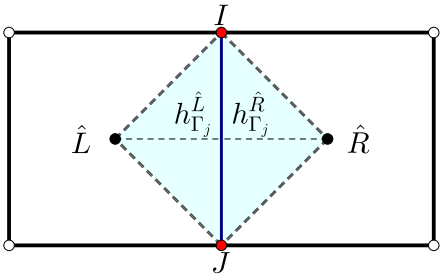

Fig. 4. Diamond stencil (light blue region) of the MPFA-D on k-orthogonal grid, $\vec{\Gamma}_j$ and $\overrightarrow{\hat{L}\hat{R}}$ are perpendicular.

The MPFA-D discretisation of the Darcy flux in equation (12) relies on pressure values calculated at the auxiliary nodes I and J that comprise the analysed face Γ_j. To overcome this problem, we define the pressure at these nodes as a linear combination of the pressure at the control volumes around these nodes. It follows:

$$p_I = \sum_{k=1}^{n_I} w_k p_k \tag{19}$$

where n_I is the number of volumes around I and w_k is the weight attributed to pressure p_k. In this work we employ the Linearity-Preserving Explicit Weighted 2 (LPEW-2) interpolation, which has been shown to be robust for simulations in anisotropic and heterogeneous media [9]. See [23,9,16] for the derivation, definition and further details of the LPEW-2 method as well as the MPFA-D formulation.

2.3. The cross diffusion terms (CDT)

By expanding the flux expression on Equation (12), we can rewrite the MPFA flux expression as it follows:

$$(\vec{v}\cdot\vec{N})_{\Gamma_j} \simeq \underbrace{\tau_{\Gamma_j}(p_{\hat{R}} - p_{\hat{L}})}_{\text{TPFA}} \quad \underbrace{- \tau_{\Gamma_j} v_{\Gamma_j}(p_J - p_I)}_{\text{Cross Diffusion Terms}} \tag{20}$$

In other words, the MPFA-D flux is a combination of the TPFA as defined on Equation (11) plus the terms responsible to capture the cross diffusion.

In flux notation this can be expressed as it follows:

$$(\vec{v}\cdot\vec{N})^{\text{MPFA}} = (\vec{v}\cdot\vec{N})^{\text{TPFA}} + (\vec{v}\cdot\vec{N})^{\text{CDT}} \tag{21}$$

Note that on a k-orthogonal grid, such as the one in Fig. 4, the permeability tensor principle axes are aligned, $\Gamma_j \perp \overrightarrow{\hat{L}\hat{R}}$ leading to $\vec{\Gamma}_j \cdot \overrightarrow{\hat{L}\hat{R}} = 0$, $K^t_{\Gamma_{j(L)}}$ and $K^t_{\Gamma_{j(R)}}$ to be 0 in Equations (15) and (16). As a consequence the non-dimensional tangential v_{Γ_j} coefficient in equation (14) is also zero in this case, reducing the MPFA-D to the standard TPFA as defined by equation (11).

It is important to note that while we employed the MPFA-D method in this work, any other linear MPFA scheme can also be formulated similarly. In situations where the flux splitting is not straightforward, you can simply subtract the standard flux expression of TPFA from a specific MPFA expression to identify the cross-diffusion terms. The definition on the cross-diffusion terms of the boundary conditions is analogous.

2.4. Matrix representation of the pressure equation

After assembling the system of equations using a consistent discrete flux approximation with the corresponding boundary conditions, we obtain a discrete version of the pressure equation (9), as it follows:

$$Mp = Q \tag{22}$$

where M denotes the transmissiblity matrix, p is the pressure vector and Q represents the source and sink term vector of a given scheme.

It is possible to write this system as the following block matrix system of equations where the Dirichlet boundary $\partial\Omega_D$ and internal volumes Ω are combined together as:

$$\begin{bmatrix} M_{\Omega\Omega} & M_{\Omega\partial\Omega_D} \\ M_{\partial\Omega_D\Omega} & M_{\partial\Omega_D\partial\Omega_D} \end{bmatrix} \begin{bmatrix} p_\Omega \\ p_{\partial\Omega_D} \end{bmatrix} = \begin{bmatrix} Q_\Omega \\ Q_{\partial\Omega_D} \end{bmatrix} \tag{23}$$

With no loss of generality we can represent the system, $Mp = Q$ as:

$$\begin{bmatrix} M_{\Omega\Omega} & M_{\Omega\partial\Omega_D} \\ 0 & I \end{bmatrix} \begin{bmatrix} p_\Omega \\ p_{\partial\Omega_D} \end{bmatrix} = \begin{bmatrix} Q_\Omega \\ g_D \end{bmatrix} \tag{24}$$

where I represents the identity matrix.

This way, the inverse of M, give in Equation (24), becomes:

$$M^{-1} = \begin{bmatrix} M_{\Omega\Omega}^{-1} & -M_{\Omega\Omega}^{-1} M_{\Omega\partial\Omega_D} \\ 0 & I \end{bmatrix} \tag{25}$$

Thus, the solution for internal control volumes p_Ω of the resulting block matrix system of equations (23) can be written as:

$$p_\Omega = M_{\Omega\Omega}^{-1}(Q_\Omega - M_{\Omega\partial\Omega_D} p_{\partial\Omega_D}) \tag{26}$$

2.5. Discrete maximum principle

Prior to introduce the Discrete Maximum Principle (DMP), we will first present theorems and definitions used to define it. Henceforth, a matrix inequality refers to an element-wise operation where all matrix entries hold the inequality unless explicitly stated otherwise.

Definition 2.2. A non-singular square matrix M is said to be monotone if for any vector x, $Mx \geq 0$ implies $x \geq 0$. In other words, a matrix is monotone if $M^{-1} \geq 0$ [36].

From equation (25), we can infer that if M^{-1} is monotone, $M_{\Omega\Omega}^{-1} > 0$, and $M_{\Omega\partial\Omega_D} < 0$.

Definition 2.3. [3] A matrix M is considered an M-matrix if the matrix is monotone (or positive-definite) with

$$m_{i,j} \leq 0 \qquad \forall i, j \quad i \neq j \tag{27}$$

Definition 2.4. A matrix M is irreducible, if there is no permutation matrix P such that [41]:

$$P^T M P = \begin{bmatrix} M_{1,1} & M_{1,2} \\ 0 & M_{2,2} \end{bmatrix} \tag{28}$$

where $M_{1,1}, M_{1,2}$ and $M_{2,2}$ are square matrices.

Theorem 2.1. *A given matrix M is an M-matrix [41,20] if*

$$\begin{aligned} &m_{i,i} > 0 \qquad \forall i \\ &m_{i,j} \leq 0 \qquad \forall i, j \quad i \neq j \\ &\Sigma_j m_{i,j} \geq 0 \qquad \forall i \end{aligned} \tag{29}$$

and M is irreducible and must be either strictly diagonally dominant (strict inequality in the latter of Eq. (29)) or weakly diagonally dominant with strict inequality for at least one row.

A consequence of the definition (2.3) is that if M is an M-Matrix, then by definition, M is also monotone. M-matrix is a desirable property because it ensures a local DMP (LDMP) [20] (discussed below) and faster convergence of iterative solvers [17,27,41].

The Discrete Maximum Principle refers to any analogous definition of the continuous maximum principle for a discrete system.

Definition 2.5. The linear system of equations (24) holds the DMP if [27]:

$$Q \geq 0 \longrightarrow p \geq 0 \tag{30}$$

while positive maxima are attained on the boundaries for $Q_\Omega \leq 0$:

$$\max_k p_k \leq \max_j \{0, g_{Dj}\} \tag{31}$$

or positive minima are attained on the boundaries for $Q_\Omega \geq 0$:

$$\min_k p_k \geq \min_j \{0, g_{Dj}\} \tag{32}$$

and if there are not source and sink terms $Q_\Omega = 0$, i.e.,

$$\min_j \{0, g_{Dj}\} \leq \min_k p_k \leq \max_j \{0, g_{Dj}\} \tag{33}$$

More details on the definition and the proofs of the theorems above can be found in [41,27]. It should be noted that DMP conditions are defined globally, i.e. where the maximum/minimum values are on the boundary. However, in [20,21] it is shown that any method with an M-matrix has a discrete solution where each discrete solution value is a convex average of its neighbours, which is consistent with the solution having no local spurious extrema. This property is referred to as a local DMP (LDMP). We note that while a LDMP ensures a global DMP the converse does not follow.

2.6. Non-linear flux limited splitting

The Flux Limited Splitting (FLS) method arises from two premises, the linear TPFA method always produces M-Matrix, and the flux expression of any CVD-MPFA scheme can be written as the sum of the TPFA term and the Cross-Diffusion terms. The idea is to limit the amount of cross-diffusion of the original CVD technique to improve or restore the DMP whilst maintaining mass conservation. We find the (LS) flux, by adding a parameter to Equation (21) that limits the cross diffusion terms for each face, as follows:

$$(\vec{v}\cdot\vec{N})^{\mathrm{FLS}}_{\Gamma_j} = (\vec{v}\cdot\vec{N})^{\mathrm{TPFA}}_{\Gamma_j} + \beta_{\Gamma_j}(\vec{v}\cdot\vec{N})^{\mathrm{CDT}}_{\Gamma_j} \tag{34}$$

where β_{Γ_j} is a relaxation parameter or a face based "flux limiter" associated with a face Γ_j in Ω that ensures the limited flux is a convex combination of the TPFA and MPFA solutions, i.e. for $\beta_{\Gamma_j}=0$ flux becomes purely TPFA, while $\beta_{\Gamma_j}=1$ recovers the standard method:

$$0 \le \beta_{\Gamma_j} \le 1 \tag{35}$$

The idea is to use the Definition 2.5 to establish an algorithm that detects control volumes violating the DMP and adjusts the non-linear parameter β_{Γ_j} to avoid this issue. However, the DMP is a property evaluated for each control volume Ω_k meanwhile β_{Γ_j} is a parameter associated with the faces Γ_j. To tackle this problem, we look back at the M-Matrix Flux Splitting method [18,31,33].

2.6.1. M-matrix flux limited splitting

The M-Matrix Flux Splitting is a technique proposed by [17] for CVD-MPFA formulations that splits the CVD-MPFA matrix in terms of TPFA and cross-diffusion terms matrices producing an iterative semi-implicit scheme driven by the TPFA matrix and ensuring mass conservation at each iteration level. In the Finite Volume context, diagonally dominant M-matrices are obtained with the most common TPFA method. Nevertheless, most problems related to petroleum reservoirs require a flux approximation that is consistent when applied to problems involving anisotropic media on general meshes [21]. The main idea of the M-Matrix Flux Splitting method is to create a semi-implicit scheme that exploits the fast convergence feature of the M-Matrix property of TPFA, where the only matrix to be inverted is a symmetric positive definite M-matrix, for both structured and unstructured grids. In addition, a key motivation is to enable standard simulators to include full-tensor problems while using the standard TPFA method solver, which also has reduced bandwidth on structured grids. The resulting framework produced results comparable to those of full matrix inversion, and eliminated $O(1)$ errors in the flow caused by the standard diagonal tensor approximation commonly employed in many existing simulators In addition, the algebraic nature of the method can be extended directly to 3-D or any different formulation [32].

To summarise this technique, let us define a linear system of equations obtained with an arbitrary CVD-MPFA method.

$$M_{\mathrm{MPFA}}p = Q_{\mathrm{MPFA}} \tag{36}$$

We can split M_{MPFA} in equation (36) in terms of M_{TPFA} and M_{CDT}, as:

$$M_{\mathrm{TPFA}}p + M_{\mathrm{CDT}}p = Q_{\mathrm{TPFA}} + Q_{\mathrm{CDT}} \quad \text{where} \quad M_{\mathrm{CDT}} = M_{\mathrm{MPFA}} - M_{\mathrm{TPFA}}, \quad Q_{\mathrm{CDT}} = Q_{\mathrm{MPFA}} - Q_{\mathrm{TPFA}} \tag{37}$$

To derive the semi-implicit scheme, we write the discrete pressure equation approximation in terms of M_{MPFA} and M_{CDT} which are approximated at different iteration levels, resulting in the following iterative method:

$$M_{\mathrm{TPFA}}p^{n+1} = Q_{\mathrm{CDT}} + Q_{\mathrm{TPFA}} - M_{\mathrm{CDT}}p^{n} \tag{38}$$

The convergence of the method is discussed [17], and the method is stable if:

$$||I - M^{-1}_{\mathrm{TPFA}}M_{\mathrm{MPFA}}||_{\infty} \le 1 \tag{39}$$

where the subscript ∞ represents the infinity norm.

2.6.2. Relaxation of the cross diffusion terms based on the M-matrix flux splitting

To obtain a relaxation of the Cross Diffusion Terms, we can premultiply Equation (38) by M^{-1}_{TPFA} and isolate p^{n+1}:

$$p^{n+1} = p_{\mathrm{TPFA}} + M^{-1}_{\mathrm{TPFA}}(Q^{n}_{\mathrm{CDT}} - M^{n}_{\mathrm{CDT}}p^{n}) \quad \text{where} \quad p_{\mathrm{TPFA}} = M^{-1}_{\mathrm{TPFA}}Q_{\mathrm{TPFA}} \tag{40}$$

Let us suppose that instead of limiting the flux, the limitation was imposed at the volume level. Therefore, we could add a relaxation parameter to the control volumes $\alpha^{n}_{\Omega_k}$ similarly to the way it was added on Equation (34). This way equation (40) becomes:

$$p^{n+1} = p_{\text{TPFA}} + A^n M^{-1}_{\text{TPFA}}(Q^n_{\text{LCDT}} - M^n_{\text{LCDT}} p^n) \quad \text{with} \quad A^n = \text{diag}\left(\begin{bmatrix} \alpha^n_{\Omega_1} & \cdots & \alpha^n_{\Omega_{n_v}} \end{bmatrix}\right) \quad \text{where} \quad 0 \le \alpha^n_{\Omega_n} \le 1 \tag{41}$$

in which M^n_{LCDT} represents the Limited Cross Diffusion Matrix for an iteration level n, i.e., the Cross Diffusion Terms obtained by assembling the matrix using Equation (34), and Q^n_{LCDT} the limited source and sink terms for the same iteration level. M^n_{LCDT} and Q^n_{LCDT} are defined similarly to M^n_{CDT} and Q^n_{CDT} with the exception the matrix is assembled using the flux in Equation (34).

To ensure that the Local Discrete Maximum Principle [20,21] is valid between two distinct iteration levels k and $k+1$, the following inequality must also hold for each control volume Ω_k:

$$\min(p^n_{\Omega_k}) \le p^{k+1}_{\Omega_k} \le \max(p^n_{\Omega_k}) \tag{42}$$

where $\min(p^n_{\Omega_k})$ and $\max(p^n_{\Omega_k})$ represent, respectively, the minimum and the maximum pressure values of any volume that shares at least a node with the Ω_k. Here, k stands for the inner loop counter and n the outerloop. The idea that follows while the outer loop n consists on the standard M-Matrix loop while the inner loop computes for each iteration k the relaxation parameter of the FLS $\beta^k_{\Gamma_j}$ that brings $p^k_{\Omega_k}$ closer to the boundaries of the DMP, as stated on Equation (41). Pressure $p^n_{\Omega_k}$ is only updated when we find $p^k_{\Omega_k}$ that obeys Equation (41).

If we set $p^n = p^k$, and expand p^{n+1} using the definition given in equation (40):

$$\min(p^n_{\Omega_k}) \le p_{\text{TPFA},\Omega_k} + \alpha_{\Omega_k} W_{\Omega_k} \le \max(p^n_{\Omega_k}) \quad \text{with} \quad W_{\Omega_k} = [M^{-1}_{\text{TPFA}}(Q^n_{\text{LCDT}} - M^n_{\text{LCDT}} p^n)]_{\Omega_k} \tag{43}$$

where p_{TPFA,Ω_k} represents the TPFA pressure solution for the CV Ω_k.

After some algebraic manipulation, we obtain the following interval in which α_{Ω_k} ensures that $p^n_{\Omega_k}$ satisfies the DMP:

$$L_{\Omega_k} : \begin{cases} \dfrac{\min(p^n_{\Omega_k}) - p_{\text{TPFA},\Omega_k}}{W_{\Omega_k}} \le \alpha_{\Omega_k} \le \dfrac{\max(p^n_{\Omega_k}) - p_{\text{TPFA},\Omega_k}}{W_{\Omega_k}} & W_{\Omega_k} \ge 0 \\ \dfrac{\max(p^n_{\Omega_k}) - p_{\text{TPFA},\Omega_k}}{W_{\Omega_k}} \le \alpha_{\Omega_k} \le \dfrac{\min(p^n_{\Omega_k}) - p_{\text{TPFA},\Omega_k}}{W_{\Omega_k}} & W_{\Omega_k} < 0 \end{cases} \tag{44}$$

Note that by definition:

$$W = p^{k+1} - p_{\text{TPFA}} \tag{45}$$

This way, $W_{\Omega_k} = 0$, only if $p^{k+1}_{\Omega_k} = (p_{\text{TPFA}})_{\Omega_k}$. In cases that the interval calculated on L_{Ω_k} is not physical, we limit each interval with:

$$K_{\Omega_k} : L_{\Omega_k} \cap [0,1] \tag{46}$$

We define the control volume relaxation parameter as:

$$\alpha_{\Omega_k} = \begin{cases} \max(K_{\Omega_k}) & K_{\Omega_k} \neq \varnothing \\ 1 & K_{\Omega_k} = \varnothing \end{cases} \tag{47}$$

To obtain a relaxation parameter for the face Γ_j, as required by Equation (34), we use the following relation:

$$\beta^k_{\Gamma_j} = \min(\alpha^n_L, \alpha^n_R) \tag{48}$$

where L and R represent respectively, the control volumes that are at the left and at the right sides of face Γ_j.

The inner loop is calculated as it follows:

$$p^{k+1} = p_{\text{TPFA}} + M^{-1}_{\text{TPFA}}(Q^k_{\text{LCDT}} - M^k_{\text{LCDT}} p^k) \tag{49}$$

For each k limitation procedure is performed and M^k_{LCDT} with a given $\beta^k_{\Gamma_j}$. Once a p^{k+1} that obeys Equation (43) is found, the inner loop ends and we set $\beta^n_{\Gamma_j} = \beta^k_{\Gamma_j}$ and $p^n = p^{k+1}$. The outer loops checks for convergence of p^n and if its met the procedure ends, otherwise the innter loop starts again. More details on the algorithm are found on Section 2.6.4.

2.6.3. Stability

Unlike the work of [17] that computes the solution of the MPFA system of equations using the semi-implicit relation in equation (38), the FLS system of equation is modified at every iteration. Therefore, it is natural to study the stability between two consecutive iteration levels inside the inner loop.

Let p_H be the exact solution of the implicit FLS system of equations, such that:

$$M^k_{\text{FLS}} p_H = M_{\text{TPFA}} p_H + M^k_{\text{LCDT}} p_H = Q_{\text{TPFA}} + Q_{\text{LCDT}} \tag{50}$$

If we subtract Equation (50) from the semi-implicit iteration of the FLS in Equation (49), we have:

$$M_{\text{TPFA}} e^{k+1} + M_{\text{LCDT}} e^{k} = 0 \tag{51}$$

with the relative discrete solution error $e^{k+1} = p^{k+1} - p_H$ and $e^k = p^n - p_H$.

If we solve equation (51) row-wise after some algebraic manipulation, we have:

$$e^{k+1} = M_{\text{TPFA}}^{-1} M_{\text{LCDT}}^{n} e^{k} \tag{52}$$

A method is known to be stable if its spectral radius is bounded by unity [26,17], which follows:

$$||M_{\text{TPFA}}^{-1} M_{\text{LCDT}}^{k}||_{\gamma} = ||I - M_{\text{TPFA}}^{-1} M_{\text{FLS}}^{k}||_{\gamma} \leq 1 \quad \text{with} \quad M_{\text{LCDT}}^{k} = M_{\text{FLS}}^{k} - M_{\text{TPFA}} \tag{53}$$

calculated using a γ norm.

The constraints imposed on β ensure that M_{FLS}^{k} is always bounded by M_{MPFA}^{k} and M_{TPFA}^{k}. Therefore, as we update β, the restrictions on the cross diffusion terms increase the overall stability of FLS as M_{FLS}^{k} becomes closer to M_{TPFA}^{k}. This increases the stability of the M-Matrix Flux Splitting, allowing our formulation to converge even in cases where the original M-Matrix Flux Splitting method would not. Note that while this relaxation controls the strength of the cross-diffusion terms subject to the conditions of a LDMP, consistency of the full-tensor pressure equation approximation is affected locally according to the amount of limitation employed.

2.6.4. Flux Limited Splitting algorithm

The Flux Limited Splitting methodology is defined by three straightforward Algorithms 1, 2, and 3. The first is the main algorithm that includes a pre-processing stage that previously computed the transmissibility matrices, source and sink terms and calls the algorithm that initializes the pressure, the flux limitation algorithm and the solver. The second is an algorithm that computes the initial guess used by the FLS algorithm in 2. It works by ensuring that the initial solution is a convex combination of both solutions, p_{MPFA} and p_{TPFA}, but maximizing the influence of the former. This is used to accelerate the convergence of the FLS iterations in cases where the MPFA-D solution contains too much spurious oscillations. The last step is the heart of the FLS method, the Flux Limitation algorithm, a set of routines described by Algorithm 3 that limits the cross-diffusion terms to mitigate the nonphysical oscillations. It is worth noting that in this step the pressure solution is calculated within a tolerance large enough to capture the violations of the DMP, but not too small to allow p to converge. After that, we use any arbitrary solver to find a solution within a given tolerance.

Algorithm 1: Flux Limitation Main Algorithm.

1 Compute: $M_{\text{TPFA}}, Q_{\text{TPFA}}, p_{\text{TPFA}}, M_{\text{MPFA}}, Q_{\text{MPFA}}, p_{\text{MPFA}}$;
2 Intialize: $p^0 \leftarrow$pressure initialization($Q_{\text{TPFA}}, p_{\text{TPFA}}, M_{\text{MPFA}}, Q_{\text{MPFA}}, p_{\text{MPFA}}$), ▷ see Algorithm 1;
3 Flux Limitation: $p^k, \beta, M_{\text{LCDT}}, Q_{\text{LCDT}} \leftarrow$FLS($Q_{\text{TPFA}}, p_{\text{TPFA}}, M_{\text{MPFA}}, Q_{\text{MPFA}}, p_{\text{MPFA}}, p^0$), ▷ see Algorithm 2;
4 Solve: $p_{\text{limited}}, (\vec{v} \cdot \vec{N}_{\text{limited}}) \leftarrow$solve($M_{\text{TPFA}}, M_{\text{LCDT}}, Q_{\text{TPFA}}, Q_{\text{LCDT}}, \beta, p^k$);

3. Results

Results produced by the Flux Limited Splitting formulations coupled with MPFA-D for simulating single-phase flows in highly heterogeneous and anisotropic media are presented below. For all tests we have used $tol = 5 \times 10^{-4}$, and for the parameter that captures the rate of residue decrease over the previous iteration, $lim = 5 \times 10^{-2}$. All simulation comparisons are made with the monotone non-linear TPFA (NL-TPFA) method [11].

3.1. Fluid flow in a domain with a square hole in a heterogeneous and extremely anisotropic medium

The first example was originally devised by Queiroz et al. [37] to study the loss of monotonicity in linear CVD-MPFA schemes when employing highly anisotropic diffusion coefficient fields. In this problem, the analyzed domain is in the form of a square $\Omega = [0,1]^2$ with a concentric opening that is also in the form of a square $\Omega = [4/9, 5/9]^2$. Dirichlet conditions are applied to the boundaries of the domain, with the outer boundaries set as $p^1 = 0$ at $\partial\Omega_1$ and the inner boundaries set as $p^2 = 2$ at $\partial\Omega_2$. The diffusion tensor is strongly anisotropic and discontinuous, and given by:

$$K(x,y) = \begin{cases} \begin{bmatrix} \cos(\pi/2) & -\sin(\pi/2) \\ sin(\pi/2) & cos(\pi/2) \end{bmatrix} \begin{bmatrix} 100 & 0 \\ 0 & 0.01 \end{bmatrix} \begin{bmatrix} \cos(\pi/2) & \sin(\pi/2) \\ -sin(\pi/2) & cos(\pi/2) \end{bmatrix} & K_1 : x \leq 0.5 \\ \begin{bmatrix} (y+\epsilon)^2 + \delta(x+\epsilon)^2 & -(1-\delta)(y+\epsilon)(x+\epsilon) \\ -(1-\delta)(y+\epsilon)(x+\epsilon) & (x+\epsilon)^2 + \delta(y+\epsilon)^2 \end{bmatrix} & K_2 : x > 0.5 \end{cases} \tag{54}$$

with $\epsilon = 10^{-3}$.

The physical domain is discretised with three different unstructured grids. The first is a coarser grid with 1,280 quadrilateral slightly distorted elements, the second is an intermediate grid with 2,678 uniform isotropic triangular elements and the last is an

Algorithm 2: Pressure Initialization Algorithm: It checks the number of Dirichlet Boundary Conditions $n(g_D)$ and the Q_s source and sink terms to find an initial guess p_{init} as close as possible to p_{MPFA} while avoiding the loss of DMP.

Input : $p_{\text{TPFA}}, p_{\text{MPFA}}$
Output: p_{init}
$pa_{min} \leftarrow \min(p_{\text{TPFA}})$;
$pa_{max} \leftarrow \max(p_{\text{TPFA}})$;
if $\max(p_{MPFA)} > pa_{max}$ **then**
  $\gamma_{max} \leftarrow$ volume where $\max(p_{\text{MPFA}})$;
end
if $\min(p_{MPFA)} < pa_{mix}$ **then**
  $\gamma_{min} \leftarrow$ volume where $\min(p_{\text{MPFA}})$;
end
if $Q_s = 0$ *and* $n(g_D) > 1$ **then**
  $\eta_1 \leftarrow \frac{pa_{max} - p_{\text{MPFA}}^{\gamma max}}{p_{\text{TPFA}}^{\gamma max} - p_{\text{MPFA}}^{\gamma max}}$ $\eta_2 \leftarrow \frac{pa_{min} - p_{\text{MPFA}}^{\gamma min}}{p_{\text{TPFA}}^{\gamma min} - p_{\text{MPFA}}^{\gamma min}}$;
  $\eta \leftarrow \frac{2}{3}\min(\eta_1, \eta_2)$;
else
  if $Q_s > 0$ **then**
    $\eta \leftarrow \frac{pa_{min} - p_{\text{MPFA}}^{\gamma min}}{p_{\text{TPFA}}^{\gamma min} - p_{\text{MPFA}}^{\gamma min}}$;
  else
    $\eta \leftarrow \frac{pa_{max} - p_{\text{MPFA}}^{\gamma max}}{p_{\text{TPFA}}^{\gamma max} - p_{\text{MPFA}}^{\gamma max}}$;
  end
  $\eta \leftarrow \frac{3}{4}\eta$;
end
$p_{init} \leftarrow (1-\eta)p_{\text{TPFA}} + \eta p_{\text{MPFA}}$;
$\theta \leftarrow$ volumes of p_{init} that violate DMP;
$p_{init}^{\theta} \leftarrow p_{\text{TPFA}}^{\theta}$

Algorithm 3: Flux Limited Splitting (FLS) Algorithm: Υ is defined number larger enough to ensure that inner and outer whiles are run at least once.

Input : $M_{\text{TPFA}}, Q_{\text{TPFA}}, p_{\text{TPFA}}, M_{\text{MPFA}}, Q_{\text{MPFA}}, p_{\text{MPFA}}, p^0$
Output: $p^n, \beta, M_{\text{LCDT}}, Q_{\text{LCDT}}$
Set: $\varepsilon \leftarrow \Upsilon$;
Set: $R_{\text{old}} \leftarrow \Upsilon$;
Initialize outer iterative counter: $n \leftarrow 1$;
Initialize outer pressure: $p_{it}^n \leftarrow p^0$;
Initialize inner pressure: $p_{it}^k \leftarrow p^0$;
while $\varepsilon \geq lim$ **do**
  Initialize inner iterative counter: $k \leftarrow 1$;
  Initialize K_{Ω_k} using Equation (44) and p_{it}^n ;
  while p_{it}^n *does not obeys DMP or* $k \leq 30$ **do**
    Initialize inner pressure: $p_{it}^k \leftarrow p^n$;
    Compute for each Ω_k: α_{Ω_k} ⊳ see section 2.6.2 ;
    Compute for each Γ_j: β_{Γ_j} ⊳ see section 2.6.2 ;
    Using β_{Γ_j} compute: $M_{\text{LCDT}}, Q_{\text{LCDT}}$;
    Solve Equation (49): $M_{\text{TPFA}} p_{it}^{n+1} = Q_{\text{TPFA}} + Q_{\text{LCDT}}^n - M_{\text{LCDT}}^n p^n$;
  end
  Reset k: $k \leftarrow 1$;
  Calculate the residue: $R_{\text{new}} \leftarrow ||(M_{\text{TPFA}} + M_{\text{LCDT}})p^k - (Q_{\text{TPFA}} + Q_{\text{LCDT}})||_2$;
  Set: $p_{it}^n \leftarrow p_{it}^k$;
  Update: $\varepsilon \leftarrow \frac{R_{\text{new}} - R_{\text{old}}}{R_{\text{old}}}$;
  Update: $R_{\text{old}} \leftarrow R_{\text{new}}$;
end

extremely fine grid with 10,712 triangular elements. These meshes were generated to evaluate the FLS under different refinements with meshes elements misaligned with the fluxes. For the sake of comparison, we ran a simulation for each of these grids with four different schemes, the FLS coupled with the MPFA-D, the linear MPFA-D, a positive-preserving monotone nonlinear TPFA (NL-TPFA) [11] and the standard linear TPFA (L-TPFA). The first grid used is the coarser grid, one can already see the advantages of the Flux Limited Splitting in comparison to the other methods. See Fig. 5. While the MPFA-D had qualitatively a good solution, the method produced a strong undershoot and a small overshoot as shown in Table 1. The L-TPFA solution produced a result that is consistent with the Discrete Maximum Principle, but is quite diffusive and does not represent the physics of the problem. The pressure field of the NL-TPFA complied with the DMP as expected, without the large amounts of diffusion that occur in the L-TPFA solution. This pattern of L-TPFA is observed throughout all the examples in this work. The Flux Limited Splitting coupled with the MPFA-D solution, in turn, fixes the overshoot and undershoot problems of the linear MPFA-D solution. It is possible to

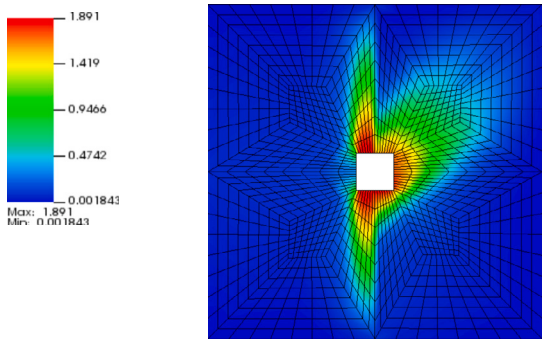

(a) FLS + MPFA-D solution.

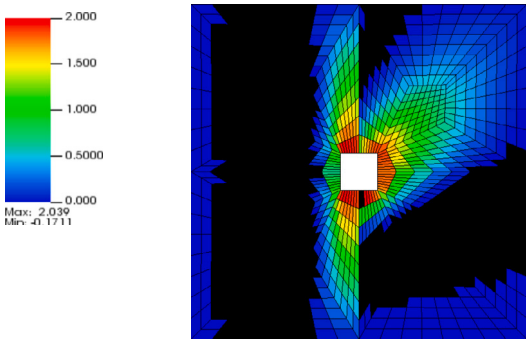

(b) Linear MPFA-D solution. Black volumes violate DMP.

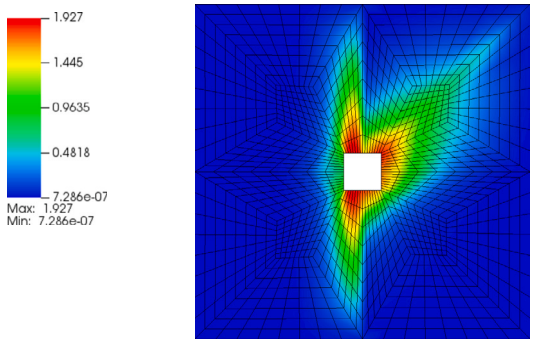

(c) NL-TPFA converged with 36 iterations.

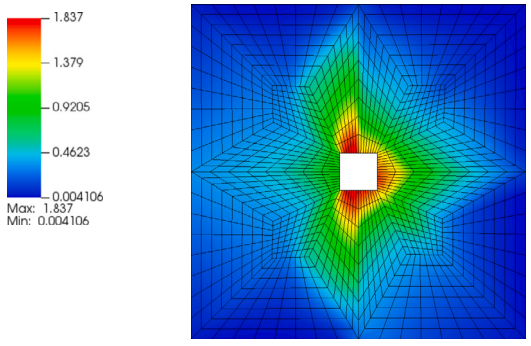

(d) L-TPFA solution.

Fig. 5. Fluid flow in a domain with a square hole in a heterogeneous and extremely anisotropic medium using a coarse grid with 1,280 quadrilateral elements.

Table 1
Maximum pressure, p_{max} and minimum pressure, p_{min} for the fluid flow in a heterogenous domain with a square hole in an extremely anisotropic media example.

	L-TPFA		MPFA-D		FLS + MPFA-D		NL-TPFA	
	p_{min}	p_{max}	p_{min}	p_{max}	p_{min}	p_{max}	p_{min}	p_{max}
Coarse grid with quadrilateral CVs	0.005	1.837	-1.711E-01	2.039	0.001849	1.891	7.286E-07	1.927
Intermediate grid with triangular CVs	8.432E-05	1.985	-1.139	2.099	2.422E-06	1.977	2.871-12	2.151
Refined grid with triangular CVs	4.192E-05	1.986	0.324	2.214	6.928E-06	1.999	0.000	3.137

see the similarity between the NL-TPFA and the FLS + MFPA-D solution, despite two main differences. The first main difference is the discontinuity on the left side of the inner boundary. While the linear MPFA-D, the NL-TPFA and the linear TPFA produce solutions with a smooth pressure distribution, the FLS + MFPA-D solution produces an area of near zero pressure in this part of the region. The second difference is seen in the pressure distribution next to the upper right corner, where the NL-TPFA produces a region resembling a channel with high permeability. This pattern could not be observed with the linear MPFA-D and Flux-Splitting + MPFA-D solutions.

On the intermediate and finer grids, the FLS + MPFA-D behaved similarly, using the triangular grids and despite the huge undershoot of the linear MPFA-D solutions as shown in Figs. 6 and 7. For both grids, the NL-TPFA approximation has either not converged or lost consistency creating a solution that violates the DMP even after several iterations. The zero pressure region next to the left inner boundary appeared to be smoothed on the FLS + MPFA-D solution for both of these grids.

It is also interesting to see how the Flux Limitation Algorithm influences the maximum and minimum pressure values for each iteration throughout the simulation. At the beginning of the simulation the Algorithm 1 calculates a pressure solution that maximizes the influence of p_{MPFA} but ensuring that no overshoot or undershoot is observed. This way, save for a very limited number of iterations, no violation of the LDMP can be observed. In terms of computational cost, this was the most demanding example. Even for a more refined grid that containing 10,712 triangular control volumes the linear MFPA-D simulation containing the pre-processing stage took 3.73 seconds while the FLS + MPFA-D counterpart took 13.25 seconds. In other words, simulating using the FLS + MPFA-D takes the time of performing 3.55 linear MPFA-D simulations. It is worth highlighting that the pre-processing stage took only 0.60 seconds. Moreover, throughout the limitation procedure shown in Fig. 8 the DMP also satisfied during all iterations.

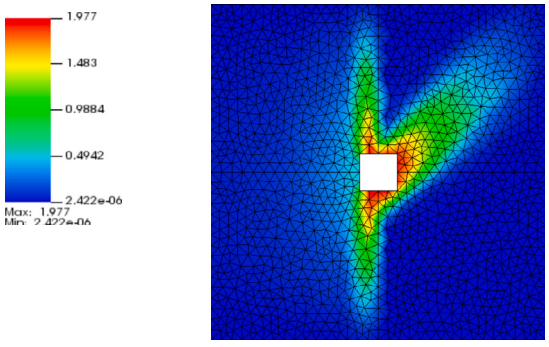

(a) FLS + MPFA-D.

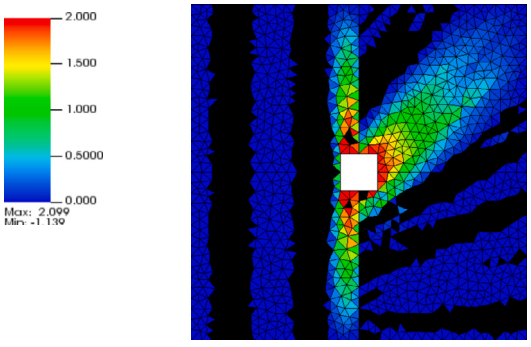

(b) Linear MPFA-D solution. Black volumes violate DMP.

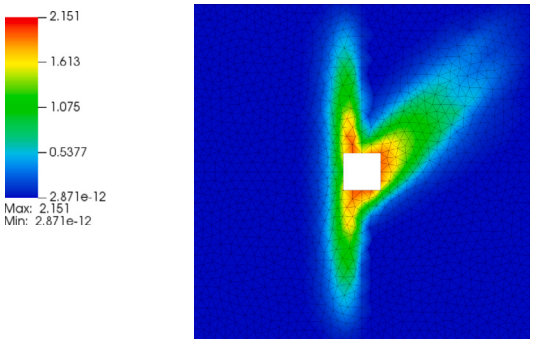

(c) NL-TPFA failed to converge: Pressure solution with 2,000 iterations.

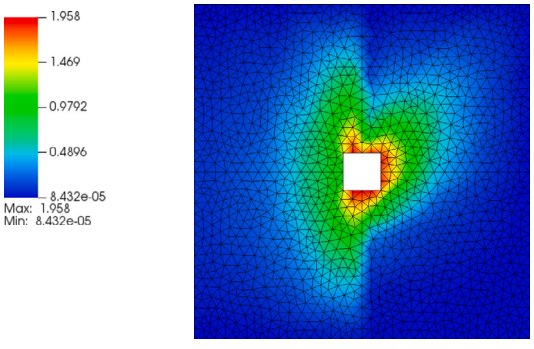

(d) L-TPFA solution.

Fig. 6. Fluid flow in a domain with a square hole in a heterogeneous and extremely anisotropic medium using an intermediate grid with 2,678 triangular elements.

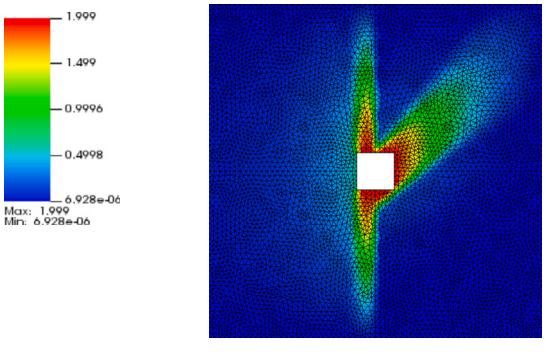

(a) FLS + MPFA-D solution.

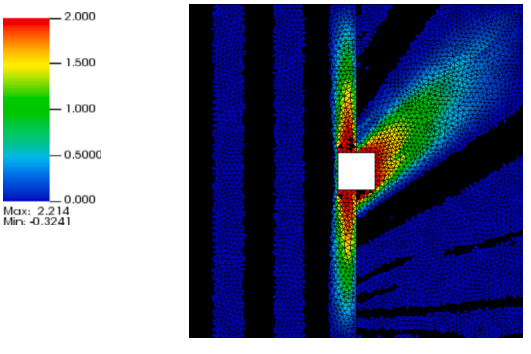

(b) Linear MPFA-D solution. Black volumes violate DMP.

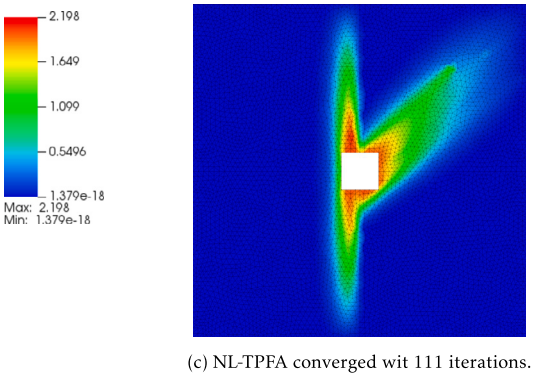

(c) NL-TPFA converged wit 111 iterations.

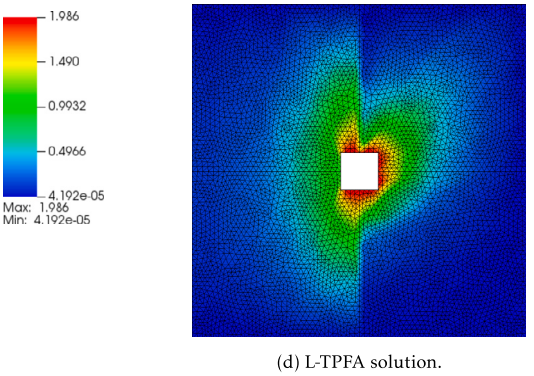

(d) L-TPFA solution.

Fig. 7. Fluid flow in a domain with a square hole in a heterogeneous and extremely anisotropic medium using a more refined grid with 10,712 triangular elements.

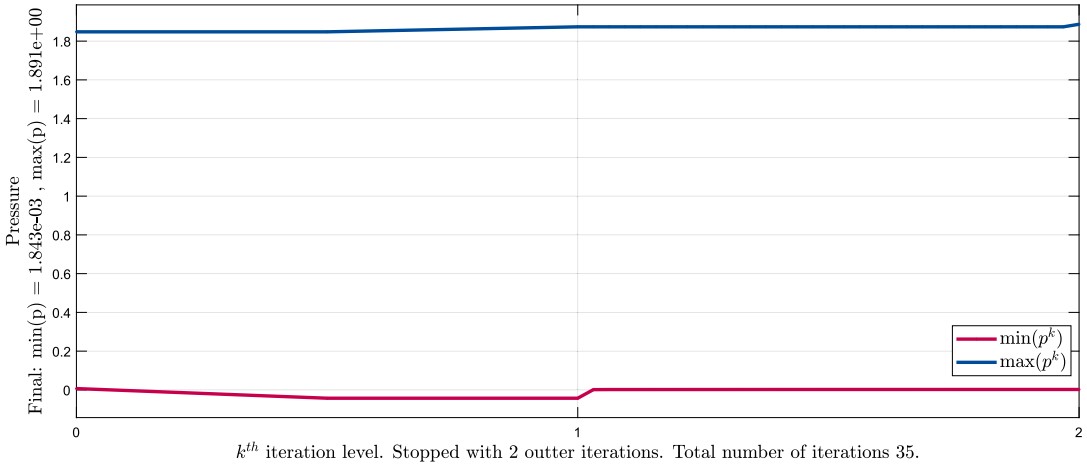

(a) Coarse Grid.

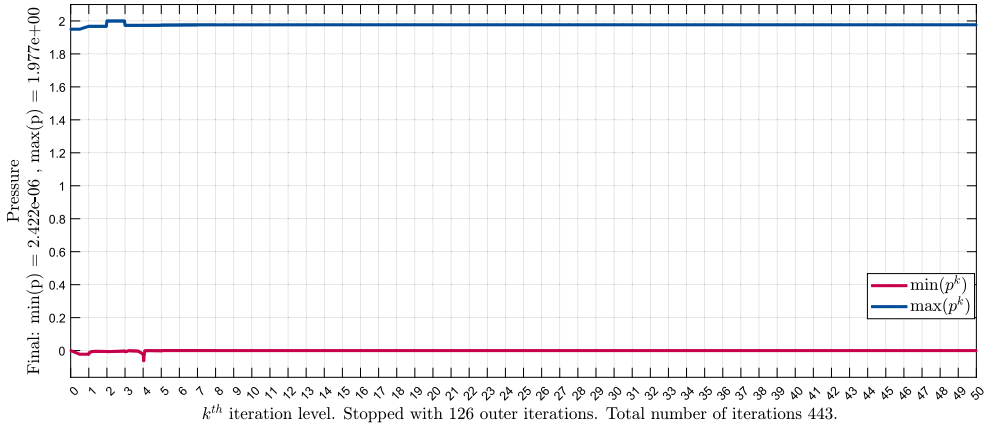

(b) Intermediate Grid.

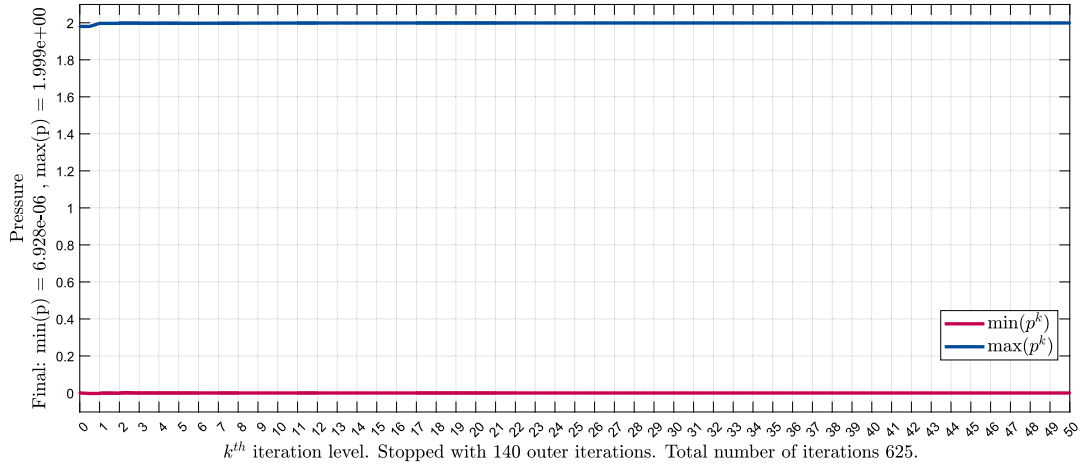

(c) Refined Grid.

Fig. 8. Flux Limitation: Maximum and minimum pressure - $p_{\max}$ and $p_{\min}$ on the example fluid flow in a domain with a square hole in a heterogeneous and extremely anisotropic medium.

Table 2
Maximum p_{max} and minimum p_{min} pressure for the fluid flow in a highly anisotropic and heterogeneous reservoir example.

	L-TPFA		Linear MPFA-D		FLS + MPFA-D		NL-TPFA	
	p_{min}	p_{max}	p_{min}	p_{max}	p_{min}	p_{max}	p_{min}	p_{max}
Structured grid	0.001	1.147	-1.033E-04	1.638	2.138E-05	1.586	8.919E-12	1.863
Distorted grid	4.908E-04	1.189	-9.389E-05	1.665	9.723E-0.6	1.626	1.437E-19	1.854
Unstructured grid	4.473E-05	1.270	-2.776E-07	1.677	6.680E-06	1.661	4.714E-16	1.945

3.2. Fluid flow in a highly anisotropic and heterogeneous reservoir

The next example was originally proposed by Lipnikov et al. [29] to evaluate the robustness of the positive preserving finite volume methods. The problem consists of a unitary quadratic domain $\Omega = [0,1]^2$ whose boundaries are subject to a prescribed pressure ($p = 0$), and into which a unitary source term is injected in a concentric square as defined by:

$$f(x,y) = \begin{cases} 1 & (x,y) \in \left[\frac{3}{8} \ \frac{5}{8}\right]^2; \\ 0, & (x,y) \notin \left[\frac{3}{8} \ \frac{5}{8}\right]^2 \end{cases} \tag{55}$$

The permeability field of the media is highly heterogeneous and anisotropic, and defined as follows:

$$\overline{K} = \begin{bmatrix} y^2 + \epsilon x^2 & -(1-\epsilon)xy \\ -(1-\epsilon)xy & \epsilon y^2 + x^2 \end{bmatrix}, \quad \epsilon = 5 \times 10^{-2} \tag{56}$$

In this example, for comparison purposes the computational domain is also discretised by using three different configurations of quadrilateral grids. The first grid is a structured quadrilateral grid comprised of 1,024 control volumes, the second grid is obtained by randomly distorting the control volumes of the first grid, and the last is an unstructured mesh with 4,791 control volumes. Again, the results are compared using our Flux Limited Splitting technique (FLS-MPFA-D), the linear MPFA-D, the NL-TPFA [11] and the L-TPFA.

First we note that, in contrast to the previous example, all methods are qualitatively quite close to each other, except the L-TPFA, which once again, produced a DMP-satisfying but completely wrong solution, with a large amount of diffusion. For the three grids used in this example, the linear MPFA-D proved to be very robust, as all solutions were quite close to the NL-TPFA and FLS + MPFA-D solutions, despite a minor undershooting (see Table 2). For the structured grid on Fig. 9, the MPFA-D and FLS + MPFA-D solution are very similar. In turn, the NL-TPFA appears to have produced a slightly more accurate pressure distribution with less diffusion. While the maximum and minimum pressure values obtained with the MPFA-D and the FLS+MPFA-D remained very close to each other, the solution produced by the NL-TPFA seemed to be much more diffusive, even though only the NL-TPFA and our FLS+MPFA-D produced strictly monotone solutions for this problem. On the distorted mesh in Fig. 10, contrary to expectation, the distortions actually helped the linear MPFA-D solution perform better and reducing the undershoot. On the other hand, as expected, the FLS+MPFA-D and the NL-TPFA produced very similar solutions with no over or undershoots. Finally, on the third and finer grid, shown in Fig. 11, the pattern seen on the other two grids seems to be reinforced. The NL-TPFA solution appears more stretched and with a larger difference between the maximum and minimum pressures. Although the problem does not have a discrete maximum, the NL-TPFA seems to produce pressure solutions significantly higher than any other tested method. In summary, in this case, the FLS+MPFA-D and the NL-TPFA yielded solutions that satisfied the DMP while the linear MPFA-D did not yield monotonic solutions for all meshes used, although it clearly produced less diffusive pressure profiles. It is also clear that our FLS+MPFA-D strategy produced less diffusive and more accurate solutions than the NL-TPFA method. It is possible to notice that the FLS limitation procedure only took a few iterations to ensure that the solution was within the DMP limits. (See Fig. 12.)

3.3. Two wells with an anisotropic and rotated permeability tensor

The third example consists of a homogeneous and anisotropic medium in a uniform square domain $\Omega = [0,1]^2$ subjected to zero flux along its boundaries. The permeability tensor with an anisotropy ratio of 1.000 is rotated $3\pi/8$ counterclockwise as described in equation (57). This problem was used by [2,40] to study the loss of monotonicity in cell-centred finite volume methods using an 11 x 11 structured quadrilateral grid. Originally, the two wells were placed in specific control volumes with prescribed pressures, $p_A = 0$, $p_B = 1$. To adapt it to the context of the unstructured grid, we use the two wells whose control volume centroids are closest to the centroids of the original control volumes, as shown in Fig. 13.

$$K = \begin{bmatrix} \cos(3\pi/8) & -\sin(3\pi/8) \\ sin(3\pi/8) & cos(3\pi/8) \end{bmatrix} \begin{bmatrix} 1 & 0 \\ 0 & 10^3 \end{bmatrix} \begin{bmatrix} \cos(3\pi/8) & \sin(3\pi/8) \\ -sin(3\pi/8) & cos(3\pi/8) \end{bmatrix} \tag{57}$$

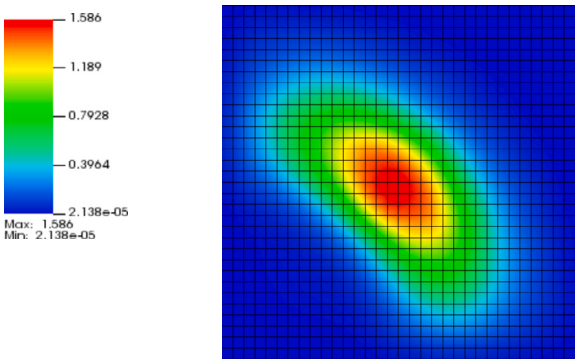

(a) FLS + MPFA-D solution.

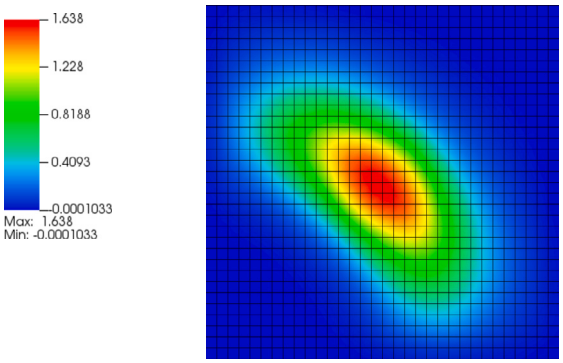

(b) Linear MPFA-D solution.

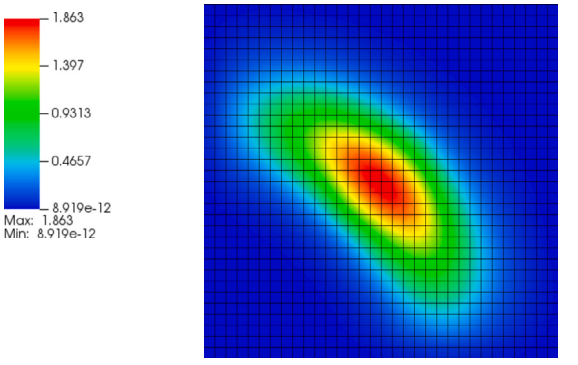

(c) NL-TPFA converged with 36 iterations.

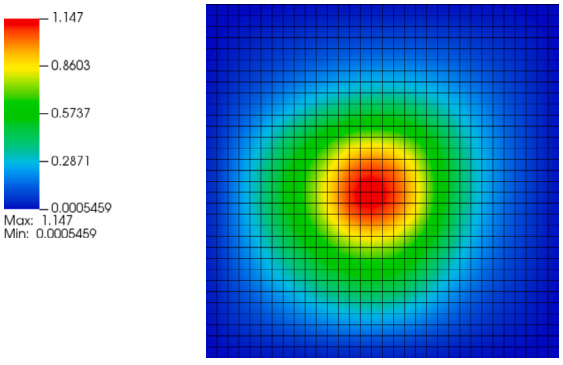

(d) L-TPFA solution.

Fig. 9. Fluid flow in a highly anisotropic and heterogeneous reservoir using a structured grid with 1,024 quadrilateral elements.

For comparison, we use four different grids in this problem. The first is the original grid, an 11x11 structured grid used [2,40]. The second is a randomly distorted version of the first grid, we also use an intermediate unstructured grid with 5,156 triangular control volumes and the last grid used is a refined unstructured grid with 20,582 triangular control volumes. Again, for each of these grids we compare the solutions using the FLS + MPFA-D, the linear MPFA-D, the NL-TPFA [11] and the standard L-TPFA.

The first noticeable difference between this problem and the previous test cases is that each method employed produces a particularly different solution with some very distinguishable features. As expected, for all meshes used the L-TPFA solution satisfies the Discrete Maximum Principle, but with excess of artificial diffusion, as previously mentioned, L-TPFA does not converge for general non k-orthogonal meshes. In turn, the NL-TPFA solution performed qualitatively well on the structured and randomly distorted quadrilateral mesh in Figs. 14 and 15, however, the method did not converge on the intermediate and refined triangular meshes presented in Figs. 16 and 17, see Table 3. It is interesting to note that the NL-TPFA produced a solution complying with the DMP for the distorted mesh, but not for the structured grid mesh. The MPFA-D also struggles with the structured mesh producing solutions with spurious oscillations (under and overshoots). Nonetheless, when the mesh was distorted and refined, these oscillations decreased. On the other hand, the FLS + MPFA-D formulation produced the more physical coherent solutions, similar to the linear MPFA-D method but with no violations of the DMP. The FLS+MPFA-D formulation produced a low and a high plateau, each with a peak and a valley bounded by the Dirichlet pressures. Once again, the FLS + MPFA-D was capable of repairing the linear MPFA-D solution by reinforcing the DMP. It is interesting to note that throughout the limitation procedure shown in Fig. 18, the DMP was also satisfied during all iterations, except for a couple of inner-iterations. Moreover we note that the simulation on the structured grid had considerably more outer iterations than even the most refined grid. We also note that the initial pressure solution proposed by Algorithm 1 violates the DMP. However, with only a few iterations the DMP was reestablished. Although there is no analytical solution for this problem, the FLS + MPFA-D formulation has consistently produced well resolved solutions representing the physics of the problem with no spurious oscillations.

3.4. Convergence test of the FLS on a distorted mesh on a reservoir with rotating anisotropy

The following problem consists on a convergence test used to assess the accuracy of non linear schemes. The problem was first introduced by [39] and later adapted by [11]. The problem itself consists in a heterogeneous reservoir with rotating anisotropy ratio. The domain is square and unitary, i.e. $[0,1]^2$ and the permeability tensor is defined by the following expression:

$$K(x,y) = R_\theta \mathrm{diag}(k_1, k_2) R_\theta^{-1} \quad \text{with} \quad \theta = 5\pi/12 \tag{58}$$

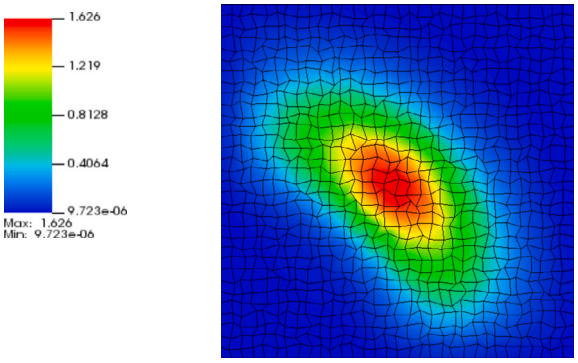

(a) FLS + MPFA-D solution.

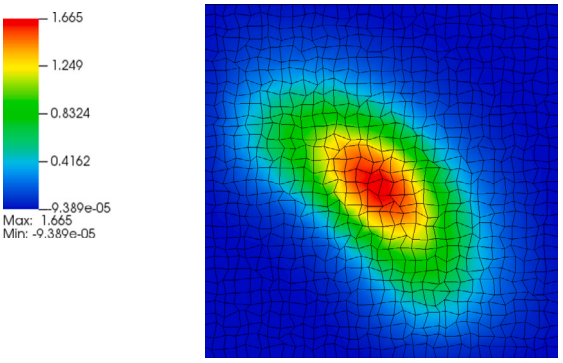

(b) Linear MPFA-D solution.

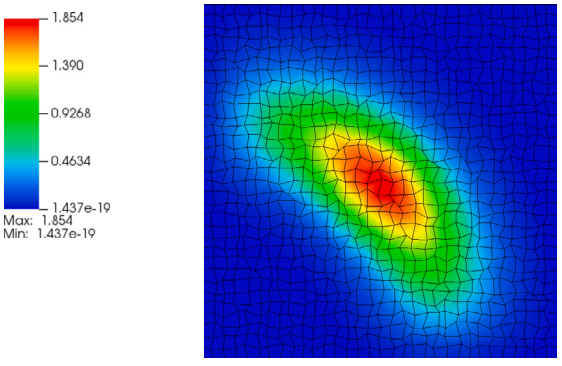

(c) NL-TPFA converged with 42 iterations.

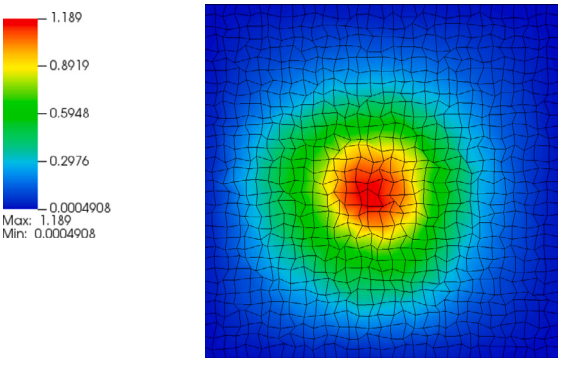

(d) L-TPFA solution.

Fig. 10. Fluid flow in a highly anisotropic and heterogeneous reservoir using a distorted quadrilateral mesh with 1,024 elements.

Table 3
Maximum p_{max} and minimum p_{min} pressures for the two wells with an anisotropic and rotated permeability tensor example.

	L-TPFA		Linear MPFA-D		FLS + MPFA-D		NL-TPFA	
	p_{min}	p_{max}	p_{min}	p_{max}	p_{min}	p_{max}	p_{min}	p_{max}
Structured Grid	0.000	1.000	-1.133E+00	2.133	0.000E+00	1.000	0.000E+00	1.642
Distorted Grid	0.000E+00	1.000	-9.137E-01	1.282	0.000E+00	1.000	0.000E+00	1.000
Unstructured Grid	0.000E+00	1.000	-2.508E-01	1.237	0.000E+00	1.000	Not converged	
Refined Unstructured Grid	0	1.000	-1.347E-01	1.030	0.000E+00	1.000	Not Converged	

where R_θ is the rotation matrix for an angle θ and diag(k_1,k_2) is a diagonal matrix defined using Equation (59).

$$k_1(x,y) = 1 + 2x^2 + y^2 \quad \text{and} \quad k_2(x,y) = 1 + x^2 + 2y^2 \tag{59}$$

The analytical solution of the problem is given by:

$$p(x,y) = \sin(\pi x)\cos \pi y \tag{60}$$

The boundary conditions are obtained by using the analytical solution on the boundaries of the domain $\delta\Omega$. The flux expression and source terms are obtained by substituting Equation (60) in Equation (1).

The obtained solution is evaluated using the L_2-norm of the errors as it follows:

$$\epsilon_p = \left(\frac{\sum_{\forall \Omega_k \in \Omega} (p(x,y) - p_k)^2 V_{\Omega_k}}{\sum_{\forall \Omega_k \in \Omega} V_{\Omega_k}} \right)^{1/2} \tag{61}$$

$$\epsilon_v = \left(\frac{\sum_{\forall \Gamma_j \in \Gamma} [(\vec{v}(x,y) - \vec{v}_k) \cdot \vec{N}]^2 A_{\Gamma_j}}{\sum_{\forall \Gamma_j \in \Gamma} A_{\Gamma_j}} \right)^{1/2} \tag{62}$$

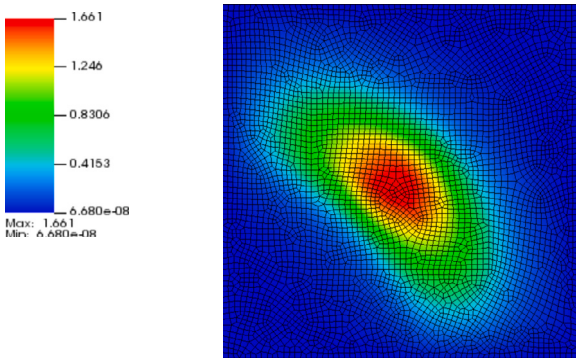

(a) FLS + MPFA-D solution.

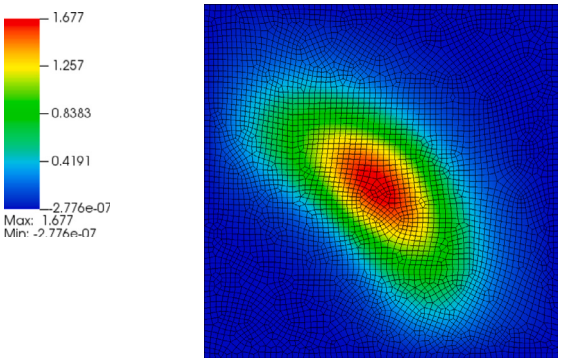

(b) Linear MPFA-D solution.

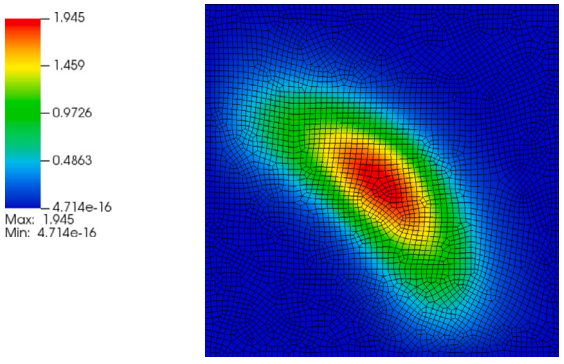

(c) NL-TPFA converged with 47 iterations.

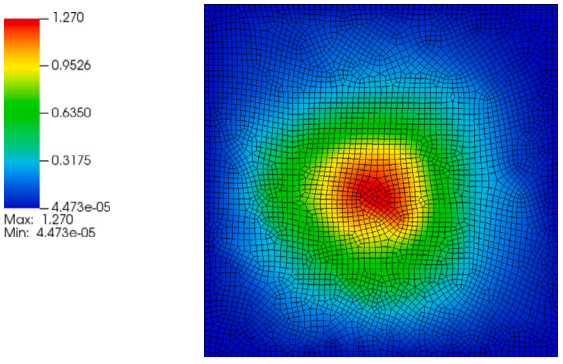

(d) L-TPFA solution.

Fig. 11. Fluid Flow in a Highly Anisotropic and Heterogeneous Reservoir using a refined quadrilateral mesh with 4,791 elements.

where ϵ_p and ϵ_v are respectively the L_2-norm of the errors of the pressure and flux, $p(x, y)$ and $\vec{v}(x, y)$ the analytical pressure and velocity calculated at the center of the control volume Ω_k and the center of the face Γ_j, respectively, and V_{Ω_k} and A_{Γ_j} represent the volume and the area of these entities.

The numerical convergence rate R_γ is obtained using the following expression:

$$R_\gamma = \frac{\log(\epsilon_\gamma^{h_2}/\epsilon_\gamma^{h_1})}{\log(h_2/h_1)} \quad \text{with} \quad \gamma = p, (\vec{v}\cdot\vec{N}) \tag{63}$$

where h_1 and h_2 denote the mesh spacing in which the latter is a more refined mesh than the former, and ϵ_γ^h is the error of the property γ calculated on a mesh h.

To evaluate the robustness of the FLS algorithm we have performed the convergence test using two sets of triangular and quadrilateral Kershaw meshes. It is possible to see that the linear MPFA-D and the FLS solutions remain very close for both triangular and quadrilateral meshes as shown in Fig. 19. In all cases, the FLS slightly shrinks the difference between the maximum and minimum values, while representing the physics of the problem. It is also possible to observe from Tables 4 and 5 that the errors and convergence rates remain almost unaffected, with the FLS actually improving the convergence of the MPFA on the triangular mesh case for both pressure and flux. The convergence rates of the pressure remained for all meshes approximately 2 and close to 1 for the velocity for the linear MPFA-D and for our new FLS methods. This indicates that our repair technique has minimal influence on the convergence rate. It is also noting that errors calculated for the Kershaw quadrilateral meshes with 36,864 and 147,456 cells, respectively, are identical for the FLS and the MPFA-D solutions. This means that for this refinements level the FLS limitation procedure was neglectful.

3.5. Linear-preserving verification

The original MPFA-D method using the LPEW-2 interpolation can reproduce piecewise linear exactly [9]. This last example was introduced to evaluate the effect of the proposed methodology on this property. The test was also introduced by [25] and adapted by [10] to test their formulations. In this test the domain is given by:

$$\Omega = \begin{cases} \Omega_1 & \forall (x,y) : \phi_1(x,y) \leq 0 \\ \Omega_2 & \forall (x,y) : \phi_1(x,y) > 0, \phi_2(x,y) < 0 \\ \Omega_3 & \forall (x,y) : \phi_2(x,y) \leq 0 \end{cases} \tag{64}$$

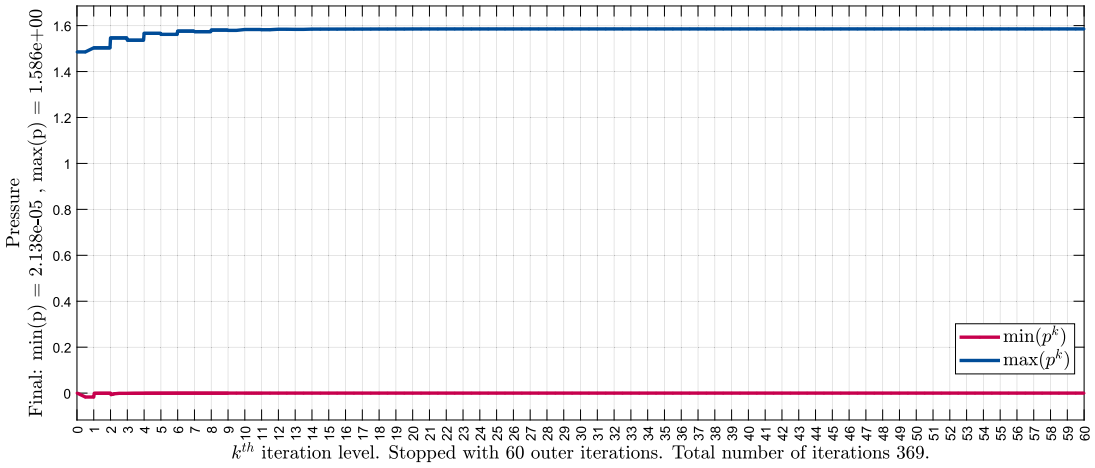

(a) Structured grid.

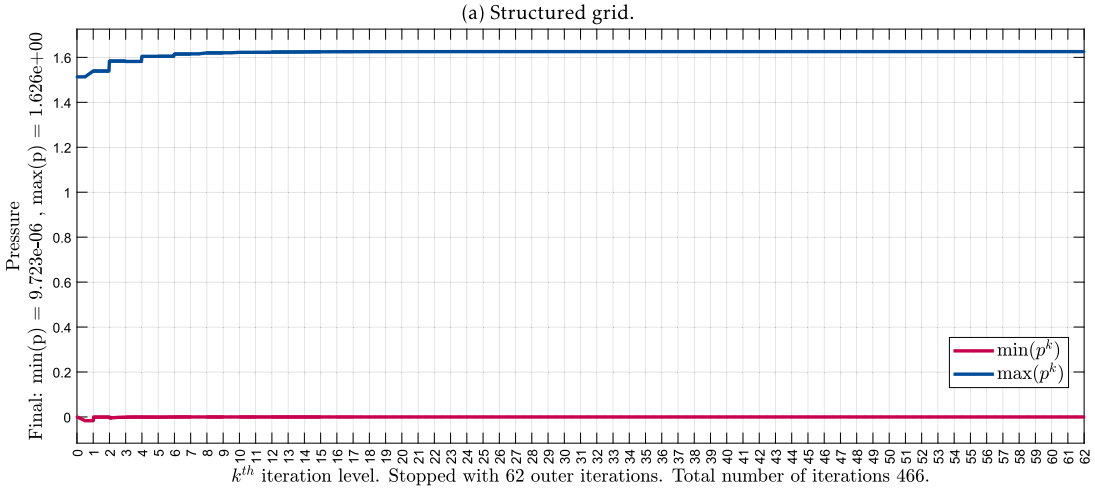

(b) Randomly distorted grid.

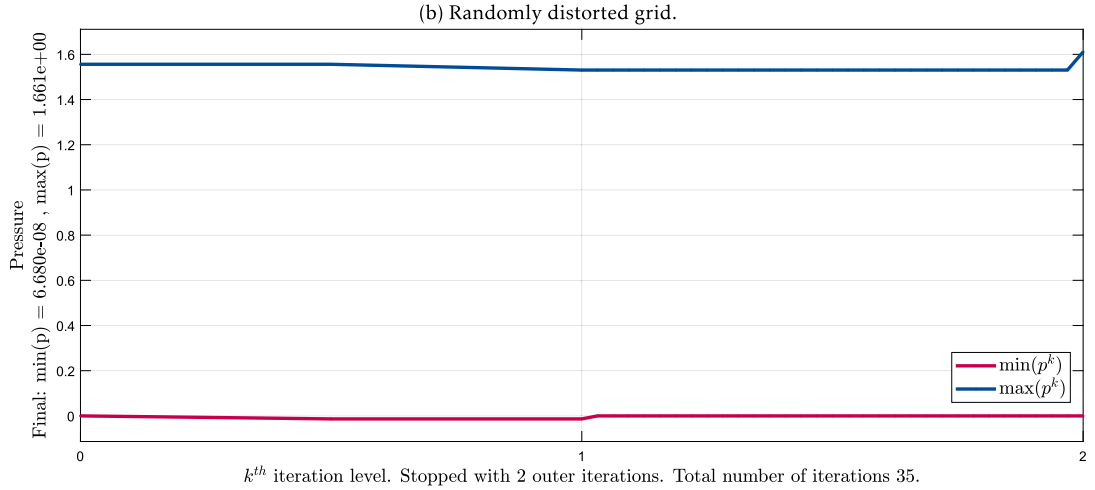

(c) Refined grid.

Fig. 12. Flux Limitation: Maximum and minimum pressure values - $p_{\max}$ and $p_{\min}$ on the example fluid flow in a highly anisotropic and heterogeneous reservoir.

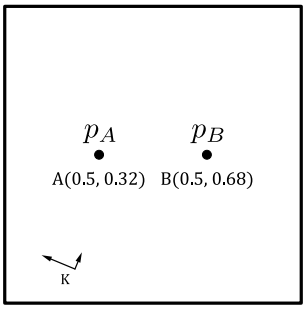

Fig. 13. Domain of the example: two wells with an anisotropic and rotated permeability tensor.

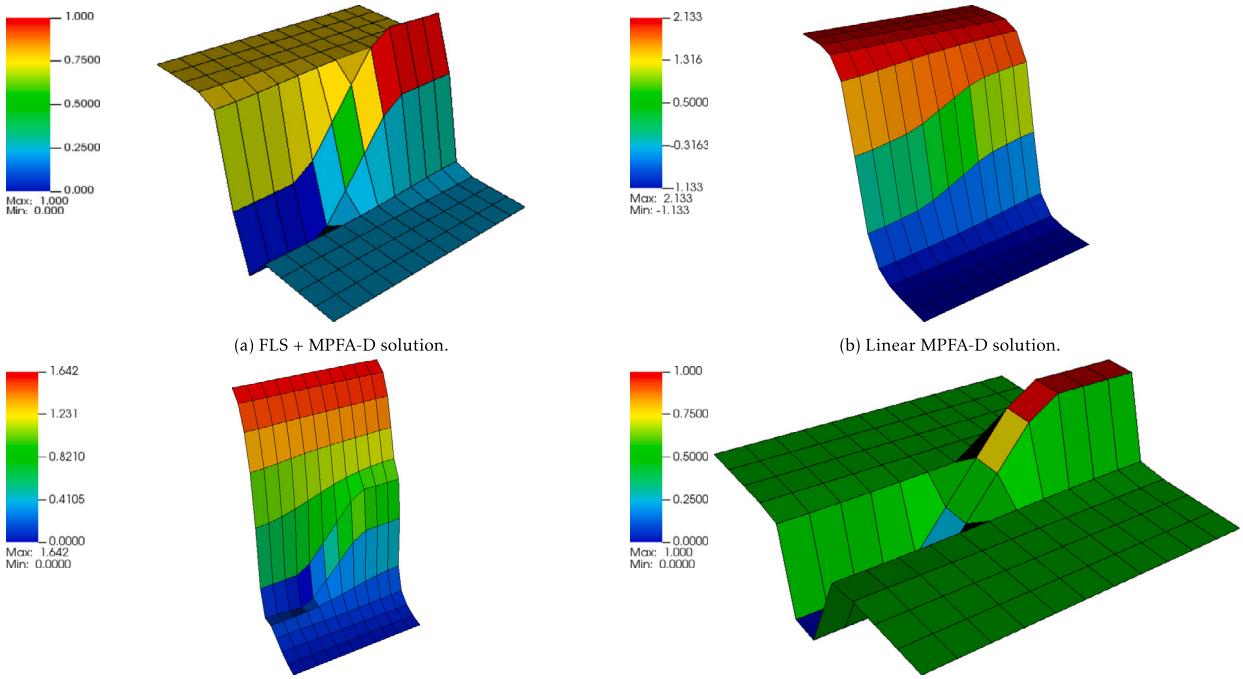

(a) FLS + MPFA-D solution.

(b) Linear MPFA-D solution.

(c) NL-TPFA converge with iterations.

(d) L-TPFA solution.

Fig. 14. Two wells with an anisotropic and rotated permeability tensor using a structured quadrilateral mesh with 11x11 elements.

Table 4
Convergence rates using the Kershaw triangular meshes.

Cells		1,152	4,608	18,432	73,728	294,912
FLS	ϵ_p	0.008568	0.00316	0.001092	0.000276	0.000054
	R_p	-	1.439010005	1.532961893	1.984206302	2.35366199
	ϵ_v	0.46978	0.257045	0.138621	0.074039	0.03445
	R_v	-	0.869949887	0.890881041	0.904776486	1.103793168
Original Linear MPFA-D	ϵ_p	0.006937	0.002477	0.000722	0.000191	0.000049
	R_p	-	1.485693324	1.77853495	1.918400692	1.962739861
	ϵ_v	0.470348	0.257201	0.138667	0.074045	0.03445
	R_v	-	0.435408922	0.891277681	0.905138237	1.103910078

where ϕ_1 and ϕ_2 are defined as:

$$\phi_1(x,y) = y - 0.2(x - 0.5) - 0.475 \quad \phi_2(x,y) = \phi_1 - 0.05. \tag{65}$$

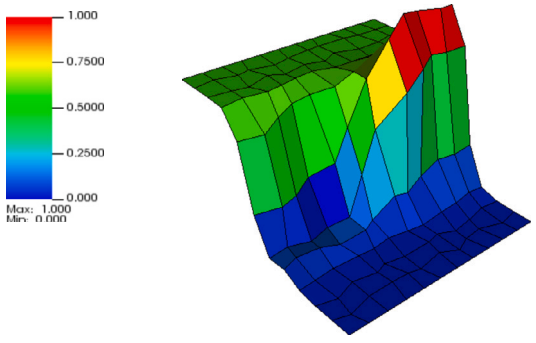

(a) FLS + MPFA-D solution.

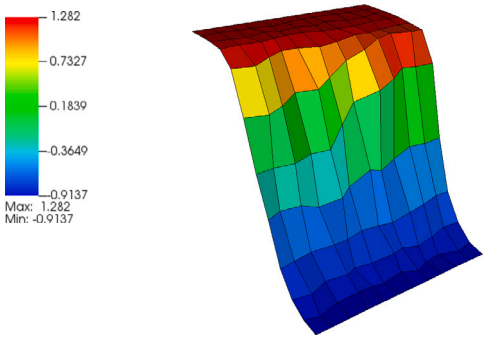

(b) Linear MPFA-D solution.

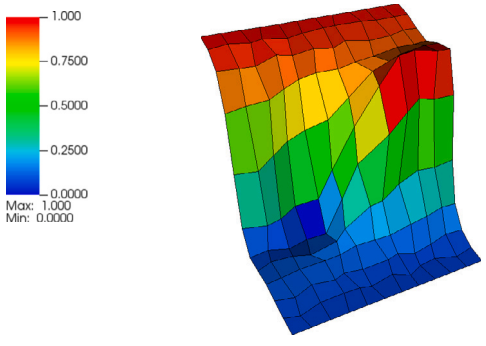

(c) NL-TPFA converged with 192 iterations.

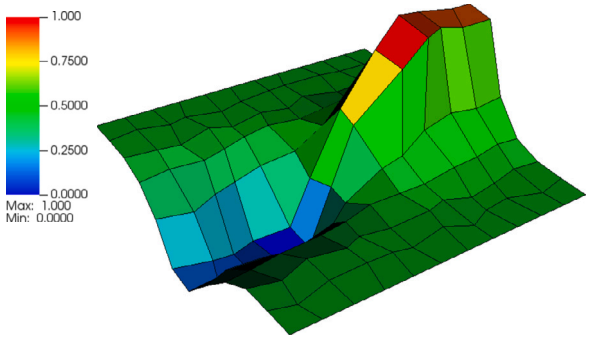

(d) L-TPFA solution.

Fig. 15. Two wells with an anisotropic and rotated permeability tensor using a randomly distorted quadrilateral mesh with 11x11 elements.

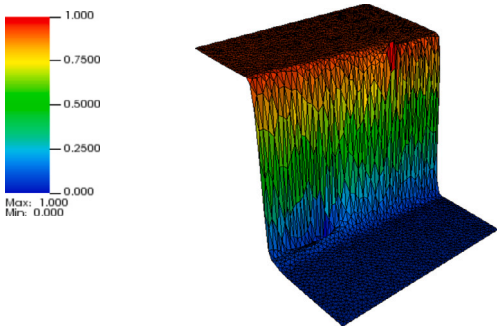

(a) FLS + MPFA-D solution.

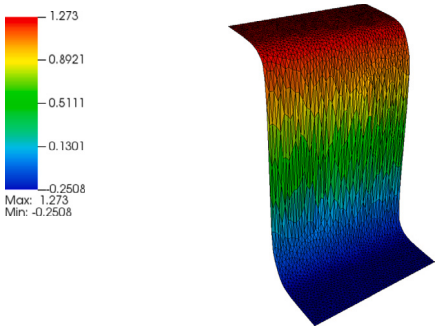

(b) Linear MPFA-D solution.

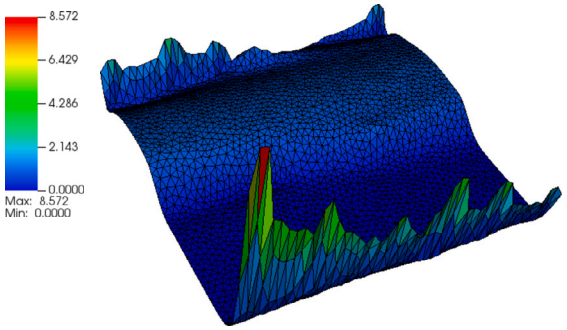

(c) NL-TPFA diverged: Pressure solution after 1,000 iterations.

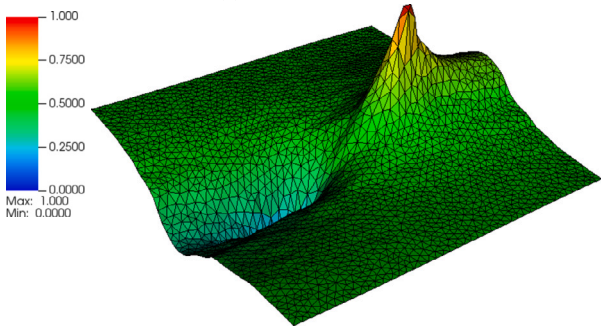

(d) L-TPFA solution.

Fig. 16. Two wells with an anisotropic and rotated permeability tensor using an intermediate unstructured mesh with 5,156 triangular elements.

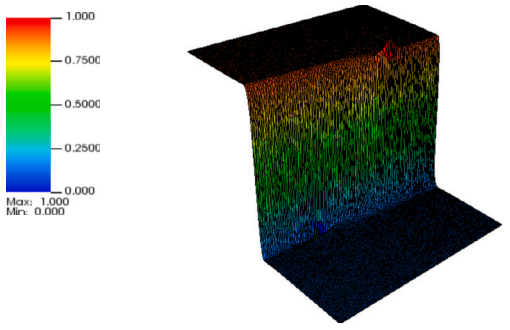

(a) FLS + MPFA-D solution.

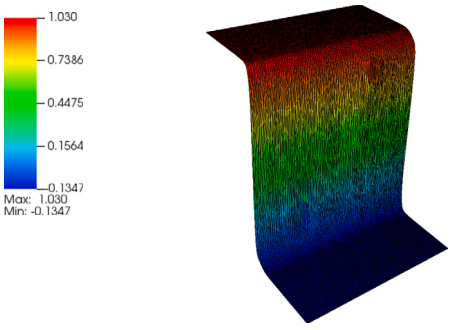

(b) Linear MPFA-D solution.

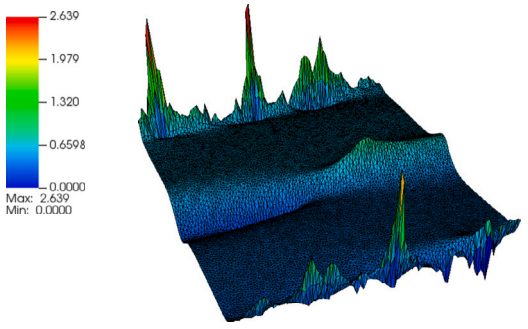

(c) NL-TPFA diverged: Pressure solution after 1,000 iterations.

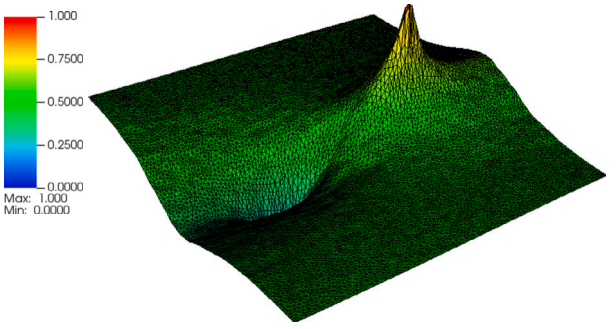

(d) L-TPFA solution.

Fig. 17. Two wells with an anisotropic and rotated permeability tensor using a refined unstructured mesh with 20,582 triangular elements.

Table 5
Convergence rates using the Kershaw quadrilateral meshes.

Cells		576	2,304	9,216	36,864	147,456
FLS	ϵ_p	0.01553	0.005438	0.001552	0.000405	0.000103
	R_p	-	1.537223242	1.808977658	1.938108976	1.975267065
	ϵ_v	0.370462	0.206202	0.102922	0.052003	0.027296
	R_v	-	0.858283942	1.00252359	0.984871544	0.929900356
Original Linear MPFA-D	ϵ_p	0.015491	0.005436	0.001551	0.000405	0.000103
	R_p	-	1.534078696	1.809376841	1.937179117	1.975267065
	ϵ_v	0.370469	0.206202	0.102922	0.052003	0.027296
	R_v	-	0.858311622	1.00252359	0.984871544	0.929900356

The permeability tensor field is given by:

$$K = \begin{cases} K_1 = R_\theta \begin{bmatrix} 100 & 0 \\ 0 & 10 \end{bmatrix} R_\theta^{-1} & \forall \Omega_k \in \Omega_1 \cup \Omega_3 \\ K_2 = R_\theta \begin{bmatrix} 1 & 0 \\ 0 & 0.1 \end{bmatrix} R_\theta^{-1} & \forall \Omega_k \in \Omega_2 \end{cases} \tag{66}$$

where R_θ is the rotation matrix for $\theta = \arctan(-0.2)$.

The simulation was performed on a quadrilateral mesh with 210 cells and the result can be seeing in Fig. 20. In order for the solution to be consistent with the simulation performed by [10], the error in this example was calculated in terms of the pressure and the velocity, instead of the flow. Therefore, we calculate the velocity error as it follows:

$$\epsilon_v = \left(\frac{\sum_{\forall \Gamma_j \in \Gamma} [(\vec{v}(x,y) - \vec{v}_k)\cdot]^2 A_{\Gamma_j}}{\sum_{\forall \Gamma_j \in \Gamma} A_{\Gamma_j}} \right)^{1/2} \tag{67}$$

The errors for the pressure field for the MPFA-D and the FLS are the same and given by, $\epsilon_p = 5.1083e-16$ while for the velocity field, we have obtained $\epsilon_v^{\text{MPFA-D}} = 4.4524e-14$ and $\epsilon_v^{\text{FLS}} = 3.7887e-14$, for the MPFA-D and the FLS, respectively. We could observe that the L_2 norm of the error in the pressure field remains identical for both MPFA-D and the FLS solution. This behaviour was also observed in the velocity with the difference in the error being also negligible. This means that the pressure solution was identical for

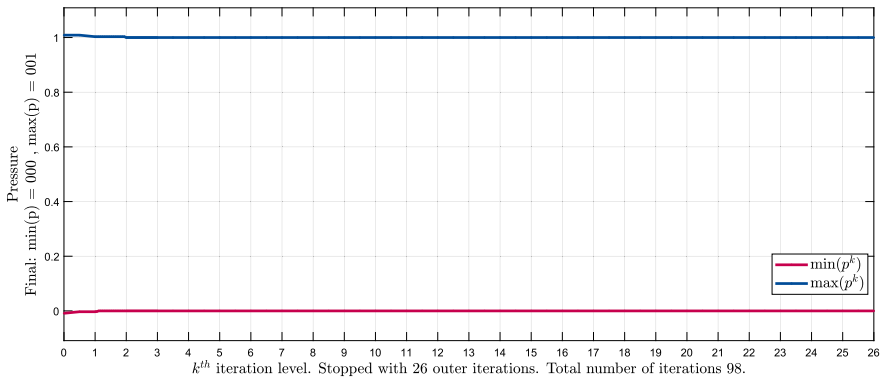

(a) Structured grid.

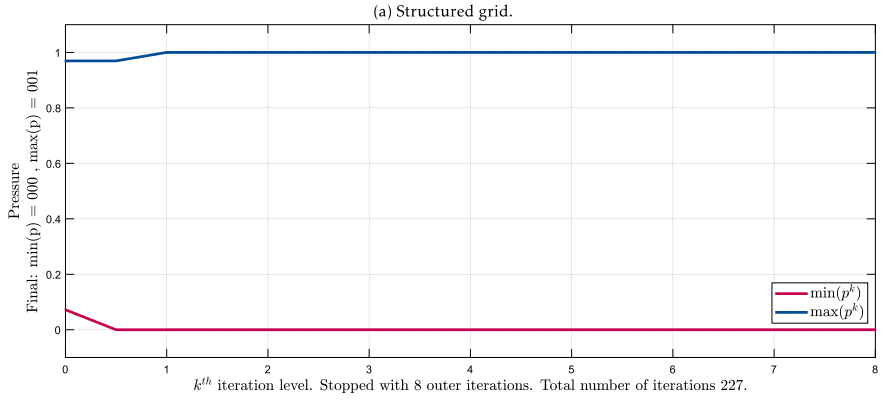

(b) Randomly distorted grid.

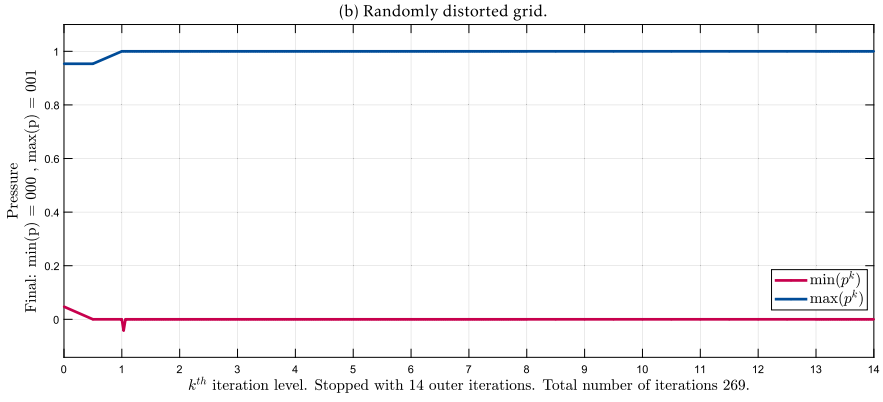

(c) Intermediate grid.

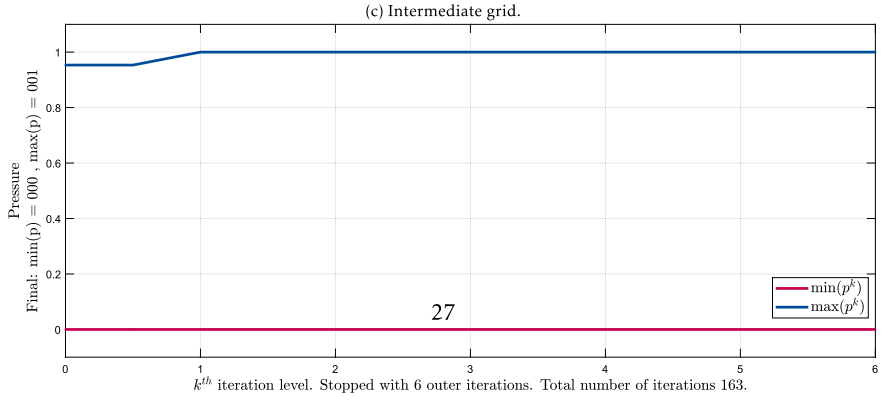

(d) Refined grid.

Fig. 18. Flux Limitation: Maximum and minimum pressure $p_{\max}$ and $p_{\min}$ on the example two wells with an anisotropic and rotated permeability tensors.

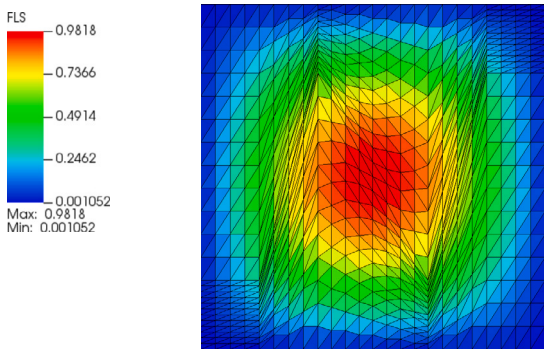

(a) FLS Solution: Triangular mesh

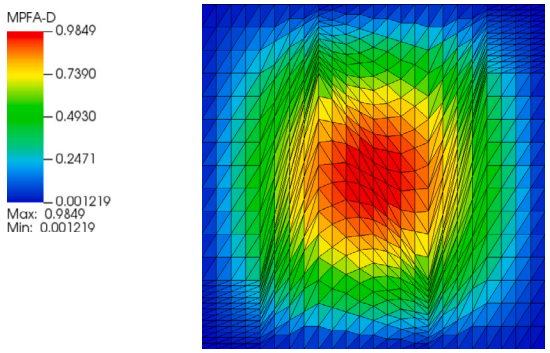

(b) Linear MPFA-D solution: Triangular mesh

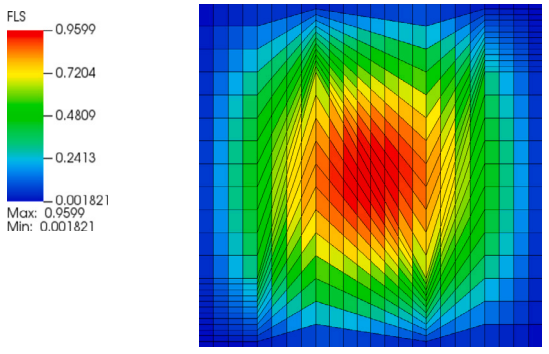

(c) FLS Solution: Quadrilateral mesh

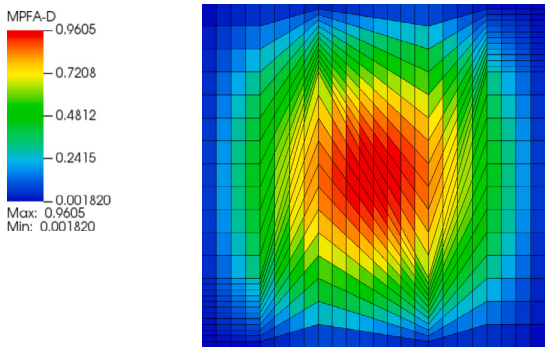

(d) Linear MPFA-D solution: Quadrilateral mesh.

Fig. 19. Convergence test of the FLS on a distorted mesh on a reservoir with rotating anisotropy: FLS and MPFA-D solutions on a Kershaw triangular mesh with 1,152 cells and on Kershaw quadrilateral mesh with 576 cells.

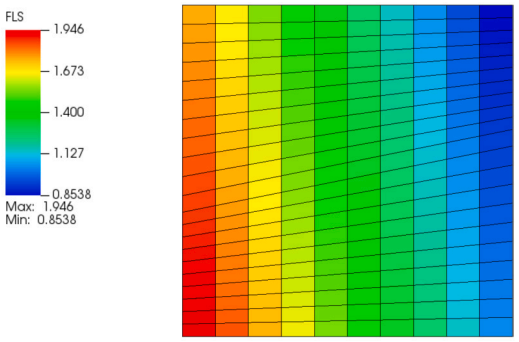

Fig. 20. Linear-Preserving verification: FLS solution on quadrilateral mesh with 210 cells.

both FLS and MPFA-D but also for the method tested in [10]. Therefore, it is possible to state that the FLS repair technique does not influence on the ability of the original MPFA-D method to reproduce piece-wise solutions exactly.

4. Conclusions

In this work we have presented a novel non-linear Flux Limited Scheme (FLS) that works as a repair technique for general linear CVD-MPFA finite volume methods. We have chosen the robust linear MPFA-D finite volume as the base scheme to build our FLS + MPFA-D formulation. The repair technique is developed based on the decomposition of the approximated flux in two parts, the TPFA and the Cross Diffusion Terms (CDT). Our algorithm is based on the M-Matrix Flux Splitting method and limits the CDT locally in regions that might otherwise introduce spurious oscillations. We have also proposed a new initialization algorithm that helped improving convergence of the iterative method even for the most challenging problems. The resulting repair technique ensures mass conservative flux solutions and is formulated using the MFPA-D method, but it can be adapted for any linear MPFA scheme. To test our new methodology we used the MPFA-D for unstructured 2-D grids using the locally conservative LPEW2 interpolation. The resulting framework was tested on benchmark problems for single-phase flows. For comparison purposes, we have presented the solutions obtained with the classical linear TPFA method, that is commonly used in petroleum reservoir simulators, the robust linear and

full pressure support MPFA-D method and the monotone NL-TPFA scheme [11]. For all cases tested, our FLS+MPFA-D formulation was able to produce solutions qualitatively very similar to the linear MPFA-D method while respecting the Local Discrete Maximum Principle (LDMP) and with much less diffusion than the monotone NL-TPFA finite volume method. The results of our formulation are at least comparable to state-of-the-art nonlinear TPFA methods, with some cases showing improved resolution and reduced computational cost. In addition, the FLS technique shows no impact on the convergence rates of the original MPFA-D scheme neither in its capability of reproducing exactly piecewise linear solutions. In conclusion, for single-phase flow problems involving severe anisotropy and heterogeneity where linear MPFA-D yields solutions with spurious oscillations, our new FLS+MPFA-D formulation maintains a LDMP and efficiently computes well resolved solutions free of spurious oscillations.

CRediT authorship contribution statement

Artur Castiel Reis de Souza: Conceptualization, Data curation, Formal analysis, Investigation, Methodology, Software, Validation, Visualization, Writing – original draft, Writing – review & editing. **Darlan Karlo Elisiário de Carvalho:** Conceptualization, Funding acquisition, Methodology, Supervision, Validation, Writing – review & editing. **Túlio de Moura Cavalcante:** Conceptualization, Investigation, Methodology, Validation, Writing – review & editing. **Fernando Raul Licapa Contreras:** Investigation, Supervision, Validation, Writing – review & editing. **Michael G. Edwards:** Conceptualization, Investigation, Methodology, Supervision, Writing – review & editing. **Paulo Roberto Maciel Lyra:** Conceptualization, Investigation, Methodology, Project administration, Resources, Supervision, Writing – original draft, Writing – review & editing.

Declaration of competing interest

The authors declare that they have no known competing financial interests or personal relationships that could have appeared to influence the work reported in this paper.

Data availability

No data was used for the research described in the article.

Acknowledgements

The authors of this paper would like to express gratitude to both Universidade Federal de Pernambuco and Swansea University, where the research work was initiated. Additionally, the authors would like to acknowledge the support received from the Science Support Foundation of the State of Pernambuco (FACEPE) under Funding Nos. IBPG-0017-3.01/18 and IBPG-0869-3.01/19, the National Council for Scientific and Technological Development (CNPq) under Funding Nos. 201099/2019-5, PQ-310145/2021-0, and PQ-308334/2019-1, the Coordination for the Improvement of Higher Education Personnel (CAPES), and the Energi Simulation Foundation for their financial support (Funding No. 53/2020) throughout this research.

References

[1] I. Aavatsmark, T. Barkve, O. Bøe, T. Mannseth, Discretization on unstructured grids for inhomogeneous, anisotropic media. Part II: discussion and numerical results, SIAM J. Sci. Comput. (1998).
[2] I. Aavatsmark, G.T. Eigestad, B.T. Mallison, J.M. Nordbotten, A compact multipoint flux approximation method with improved robustness, Numer. Methods Partial Differ. Equ. 24 (5) (2008) 1329–1360, https://doi.org/10.1002/num.20320.
[3] Axelsson Owe, Iterative Solution Methods, Cambridge University Press, Cambridge, England, March 1996.
[4] Khalid Aziz, Antonin Settari, Petroleum resevoir simulation, Appl. Sci. (1979).
[5] Clement Cances, Mathieu Cathala, Christophe Le Potier, Monotone corrections for generic cell-centered finite volume approximations of anisotropic diffusion equations, Numer. Math. 125 (3) (2013) 387–417.
[6] T.M. Cavalcante, R.J.M. Lira Filho, A.C.R. Souza, D.K.E. Carvalho, P.R.M. Lyra, A multipoint flux approximation with a diamond stencil and a non-linear defect correction strategy for the numerical solution of steady state diffusion problems in heterogeneous and anisotropic media satisfying the discrete maximum principle, J. Sci. Comput. 93 (2) (September 2022), https://doi.org/10.1007/s10915-022-01978-6.
[7] Túlio de Moura Cavalcante, Fernando Raul L. Contreras, Paulo R.M. Lyra, Darlan Karlo, E. Carvalho, A multipoint flux approximation with diamond stencil finite volume scheme for the two-dimensional simulation of fluid flows in naturally fractured reservoirs using a hybrid-grid method, Int. J. Numer. Methods Fluids 92 (10) (March 2020) 1322–1351.
[8] Qian-Yong Chen, Jing Wan, Yahan Yang, Rick T. Mifflin, Enriched multi-point flux approximation for general grids, J. Comput. Phys. 227 (3) (2008) 1701–1721, https://doi.org/10.1016/j.jcp.2007.09.021.
[9] F.R.L. Contreras, P.R.M. Lyra, M.R.A. Souza, D.K.E. Carvalho, A cell-centered multipoint flux approximation method with a diamond stencil coupled with a higher order finite volume method for the simulation of oil-water displacements in heterogeneous and anisotropic petroleum reservoirs, Comput. Fluids 127 (2016) 1.
[10] Fernando R.L. Contreras, Paulo R.M. Lyra, Darlan K.E. de Carvalho, A new multipoint flux approximation method with a quasi-local stencil (mpfa-ql) for the simulation of diffusion problems in anisotropic and heterogeneous media, Appl. Math. Model. 70 (2019) 659–676, https://doi.org/10.1016/j.apm.2019.01.033.
[11] Fernando R.L. Contreras, Darlan K.E. Carvalho, Gustavo Galindez-Ramirez, Paulo R.M. Lyra, A non-linear finite volume method coupled with a modified higher order muscl-type method for the numerical simulation of two-phase flows in non-homogeneous and non-isotropic oil reservoirs, Comput. Math. Appl. 92 (2021) 120–133.
[12] P.I. Crumpton, G.J. Shaw, A.F. Ware, Discretisation and multigrid solution of elliptic equations with mixed derivative terms and strongly discontinuous coefficients, J. Comput. Phys. 116 (2) (1995) 343–358, https://doi.org/10.1006/jcph.1995.1032.

[13] D.K.E. de Carvalho, R.B. Willmersdorf, P.R.M. Lyra, A node-centred finite volume formulation for the solution of two-phase flows in non-homogeneous porous media, Int. J. Numer. Methods Fluids 53 (8) (2007) 1197–1219, https://doi.org/10.1002/fld.1238.
[14] Darlan Karlo Elisiário de Carvalho, Ramiro Brito Willmersdorf, Paulo Roberto Maciel Lyra, Some results on the accuracy of an edge-based finite volume formulation for the solution of elliptic problems in non-homogeneous and non-isotropic media, Int. J. Numer. Methods Fluids 61 (3) (September 2009) 237–254, https://doi.org/10.1002/fld.1948.
[15] Ricardo J.M. de Lira Filho, Sidicley R. de dos Santos, Túlio de M. Cavalcante, Fernando R.L. Contreras, Paulo R.M. Lyra, Darlan K.E. de Carvalho, A linearity-preserving finite volume scheme with a diamond stencil for the simulation of anisotropic and highly heterogeneous diffusion problems using tetrahedral meshes, Computers & Structures 250 (July 2021) 106510, https://doi.org/10.1016/j.compstruc.2021.106510.
[16] Artur Castiel Reis de Souza, Lorena Monteiro Cavalcanti Barbosa, Fernando Raul Licapa Contreras, Paulo Roberto Maciel Lyra, Darlan Karlo Elisiário de Carvalho, A multiscale control volume framework using the multiscale restriction smooth basis and a non-orthodox multi-point flux approximation for the simulation of two-phase flows on truly unstructured grids, J. Pet. Sci. Eng. (May 2020).
[17] Michael G. Edwards, M-matrix flux splitting for general full tensor discretization operators on structured and unstructured grids, J. Comput. Phys. (ISSN 0021-9991) 160 (2000) 1, https://doi.org/10.1006/jcph.2000.6418.
[18] Michael G. Edwards, Unstructured, control-volume distributed, full-tensor finite-volume schemes with flow based grids, Comput. Geosci. 6 (3/4) (2002) 433–452, https://doi.org/10.1023/A:1021243231313.
[19] Michael G. Edwards, Clive F. Rogers, Finite volume discretization with imposed flux continuity for the general tensor pressure equation, Comput. Geosci. 2 (4) (1998) 259–290, https://doi.org/10.1023/a:1011510505406.
[20] Michael G. Edwards, Hongwen Zheng, A quasi-positive family of continuous Darcy-flux finite-volume schemes with full pressure support, J. Comput. Phys. 227 (22) (2008) 9333–9364.
[21] Michael G. Edwards, Hongwen Zheng, Double-families of quasi-positive Darcy-flux approximations with highly anisotropic tensors on structured and unstructured grids, J. Comput. Phys. 229 (3) (2010) 594–625, https://doi.org/10.1016/j.jcp.2009.09.037.
[22] Helmer A. Friis, Michael G. Edwards, A family of mpfa finite-volume schemes with full pressure support for the general tensor pressure equation on cell-centered triangular grids, J. Comput. Phys. 230 (1) (January 2011) 205–231, https://doi.org/10.1016/j.jcp.2010.09.012.
[23] Zhiming Gao, Jiming Wu, A linearity-preserving cell-centered scheme for the heterogeneous and anisotropic diffusion equations on general meshes, Int. J. Numer. Methods Fluids 67 (12) (2010) 2157–2183.
[24] Zhiming Gao, Jiming Wu, A small stencil and extremum-preserving scheme for anisotropic diffusion problems on arbitrary 2d and 3d meshes, J. Comput. Phys. 250 (2013) 308–331, https://doi.org/10.1016/j.jcp.2013.05.013.
[25] Raphaele Herbin, Florence Hubert, Benchmark on discretization schemes for anisotropic diffusion problems on general grids, pp. 659–692, https://www.i2m.univ-amu.fr/fvca5/benchmark/bench.pdf, December 2008.
[26] Charles Hirsch, Numerical Computation of Internal and External Flows, Wiley, 2002.
[27] D. Kuzmin, M.J. Shashkov, D. Svyatskiy, A constrained finite element method satisfying the discrete maximum principle for anisotropic diffusion problems, J. Comput. Phys. 228 (9) (2009) 3448–3463.
[28] Christophe Le Potier, Schema volumes finis monotone pour des operateurs de diffusion fortement anisotropes sur des maillages de triangles non structurés, C. R. Math. 341 (12) (2005) 787–792, https://doi.org/10.1016/j.crma.2005.10.010.
[29] K. Lipnikov, M. Shashkov, D. Svyatskiy, Yu. Vassilevski, Monotone finite volume schemes for diffusion equations on unstructured triangular and shape-regular polygonal meshes, J. Comput. Phys. 227 (1) (2007) 492–512.
[30] Shuai Miao, Jiming Wu, A nonlinear correction scheme for the heterogeneous and anisotropic diffusion problems on polygonal meshes, J. Comput. Phys. 448 (January 2022) 110729, https://doi.org/10.1016/j.jcp.2021.110729.
[31] Mayur Pal, Michael Edwards, Flux-splitting schemes for improved monotonicity of discrete solutions of elliptic equations with highly anisotropic coefficients, in: European Conference on Computational Fluid Dynamics ECCOMAS CFD 2006, 2006.
[32] Mayur Pal, Michael G. Edwards, Quasimonotonic continuous Darcy-flux approximation for general 3d grids of any element type, in: All Days, SPE, February 2007.
[33] Mayur Pal, Michael G. Edwards, Non-linear flux-splitting schemes with imposed discrete maximum principle for elliptic equations with highly anisotropic coefficients, Int. J. Numer. Methods Fluids 66 (2011) 5.
[34] Elliot Parramore, Michael G. Edwards, Mayur Pal, Sadok Lamine, Multiscale finite-volume cvd-mpfa formulations on structured and unstructured grids, Multiscale Model. Simul. 14 (2) (2016) 559–594.
[35] Christophe Le Potier, A second order in space combination of methods verifying a maximum principle for the discretization of diffusion operators, C. R. Math. 358 (1) (2020) 89–95, https://doi.org/10.5802/crmath.15.
[36] Harvey S. Price, Monotone and oscillation matrices applied to finite difference approximations, Math. Comput. 22 (103) (1968) 489–516, https://doi.org/10.1090/s0025-5718-1968-0232550-5.
[37] L.E.S. Queiroz, M.R.A. Souza, F.R.L. Contreras, P.R.M. Lyra, D.K.E. de Carvalho, On the accuracy of a nonlinear finite volume method for the solution of diffusion problems using different interpolations strategies, Int. J. Numer. Methods Fluids 74 (4) (2013) 270–291, https://doi.org/10.1002/fld.3850.
[38] Zhiqiang Sheng, Guangwei Yuan, A cell-centered nonlinear finite volume scheme preserving fully positivity for diffusion equation, J. Sci. Comput. 68 (2) (2015) 521–545, https://doi.org/10.1007/s10915-015-0148-7.
[39] Zhiqiang Sheng, Guangwei Yuan, A new nonlinear finite volume scheme preserving positivity for diffusion equations, J. Comput. Phys. 315 (June 2016) 182–193, https://doi.org/10.1016/j.jcp.2016.03.053.
[40] Kirill M. Terekhov, Bradley T. Mallison, Hamdi A. Tchelepi, Cell-centered nonlinear finite-volume methods for the heterogeneous anisotropic diffusion problem, J. Comput. Phys. 330 (2017) 245–267, https://doi.org/10.1016/j.jcp.2016.11.010.
[41] Richard S. Varga, Matrix Iterative Analysis, Springer, 2009.
[42] Jiming Wu, Zhiming Gao, Interpolation-based second-order monotone finite volume schemes for anisotropic diffusion equations on general grids, J. Comput. Phys. 275 (2014) 569–588, https://doi.org/10.1016/j.jcp.2014.07.011.
[43] Guangwei Yuan, Zhiqiang Sheng, Monotone finite volume schemes for diffusion equations on polygonal meshes, J. Comput. Phys. 227 (12) (2008) 6288–6312, https://doi.org/10.1016/j.jcp.2008.03.007.